AD-A096 145 ARIZONA UNIV TUCSON OPTICAL SCIENCES CENTER F/G 20/5
LASER GYRO THEORY EXTENSION.(U)
DEC 80 M O SCULLY F33615-79-C-1744
UNCLASSIFIED 2305 AFWAL-TR-80-1210 NL

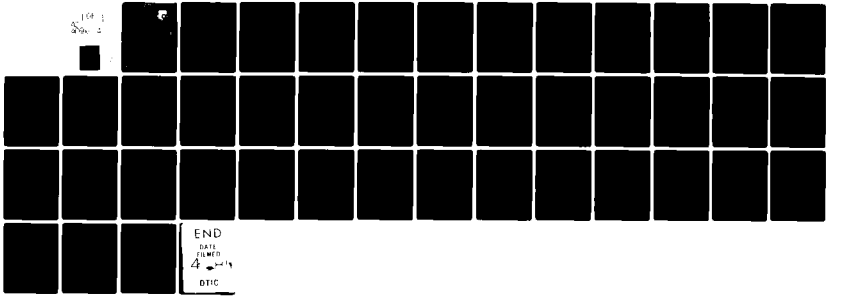

END
DATE FILMED
4-81
DTIC

LEVEL II

AFWAL-TR-80-1210

AD A096145

LASER GYRO THEORY EXTENSION

Marlan O. Scully
University of Arizona
Tucson, Arizona 85721

December 1980

TECHNICAL REPORT AFWAL-TR-80-1210

Final Report for Period 22 March 1979 to 22 September 1980

Approved for public release; distribution unlimited.

AVIONICS LABORATORY
AIR FORCE WRIGHT AERONAUTICAL LABORATORIES
AIR FORCE SYSTEMS COMMAND
WRIGHT-PATTERSON AIR FORCE BASE, OHIO 45433

NOTICE

When Government drawings, specifications, or other data are used for any purpose other than in connection with a definitely related Government procurement operation, the United States Government thereby incurs no responsibility nor any obligation whatsoever; and the fact that the government may have formulated, furnished, or in any way supplied the said drawings, specifications, or other data, is not to be regarded by implication or otherwise as in any manner licensing the holder or any other person or corporation, or conveying any rights or permission to manufacture use, or sell any patented invention that may in any way be related thereto.

This report has been reviewed by the Office of Public Affairs (ASD/PA) and is releasable to the National Technical Information Service (NTIS). At NTIS, it will be available to the general public, including foreign nations.

This technical report has been reviewed and is approved for publication.

David W. Pleva

DAVID W. PLEVA, Project Engineer

Robert E. Witters

ROBERT E. WITTERS, Technical Manager

FOR THE COMMANDER

Raymond E Siferd

RAYMOND E. SIFERD, COL, USAF
Chief, System Avionics Division
Avionics Laboratory

"If your address has changed, if you wish to be removed from our mailing list, or if the addressee is no longer employed by your organization please notify AFWAL/AAAN-2 *W-PAFB, OH 45433 to help us maintain a current mailing list".*

Copies of this report should not be returned unless return is required by security considerations, contractual obligations, or notice on a specific document.

SECURITY CLASSIFICATION OF THIS PAGE (When Data Entered)

REPORT DOCUMENTATION PAGE	READ INSTRUCTIONS BEFORE COMPLETING FORM
1. REPORT NUMBER: AFWAL-TR-80-1210	2. GOVT ACCESSION NO.: AD-A046 145
3. RECIPIENT'S CATALOG NUMBER:	
4. TITLE (and Subtitle): LASER GYRO THEORY EXTENSION.	5. TYPE OF REPORT & PERIOD COVERED: Final Scientific Report, 22 Mar 79-22 Sep 80
	6. PERFORMING ORG. REPORT NUMBER:
7. AUTHOR(s): Marlan O. Scully*	8. CONTRACT OR GRANT NUMBER(s): F33615-79-C-1744
9. PERFORMING ORGANIZATION NAME AND ADDRESS: University of Arizona, Optical Sciences Center, Tucson, Arizona 85721	10. PROGRAM ELEMENT, PROJECT, TASK AREA & WORK UNIT NUMBERS: PE 61102 F, Project 2305 R3 06
11. CONTROLLING OFFICE NAME AND ADDRESS: Avionics Laboratory (AFWAL/AAAN-2), Air Force Wright Aeronautical Laboratories, Wright-Patterson AFB, Ohio 45433	12. REPORT DATE: December 1980
	13. NUMBER OF PAGES: 40
14. MONITORING AGENCY NAME & ADDRESS (if different from Controlling Office)	15. SECURITY CLASS. (of this report): Unclassified
	15a. DECLASSIFICATION/DOWNGRADING SCHEDULE

16. DISTRIBUTION STATEMENT (of this Report)

Approved for public release; distribution unlimited

17. DISTRIBUTION STATEMENT (of the abstract entered in Block 20, if different from Report)

18. SUPPLEMENTARY NOTES

*Present Address: University of New Mexico, Institute for Modern Optics, Department of Physics and Astronomy, 800 Yale Blvd., NE, Albuquerque, New Mexico 87131

19. KEY WORDS (Continue on reverse side if necessary and identify by block number)

Zeeman laser gyro theory, laser gyro theory

20. ABSTRACT (Continue on reverse side if necessary and identify by block number)

Three investigations have been completed under the contract entitled "Laser Gyro Theory Extension," as follows: (1) The accuracy of the Zeeman laser gyro (ZLAG) theory was tested by comparing its predictions with experimental results. (2) Other multioscillator approaches to solving the lock-in problem have been investigated. (3) Two earthbound experiments to test general and special relativity theories were designed, based on the Sagnac interferometer.

DD FORM 1 JAN 73 1473

SECURITY CLASSIFICATION OF THIS PAGE (When Data Entered)

CONTENTS

I. INTRODUCTION 1

II. ZEEMAN LASER GYRO 1

III. "2+2" GYRO 2

IV. APPLICATION OF LASER ROTATIONAL SENSORS TO PROBLEMS IN GENERAL AND SPECIAL RELATIVITY 4

V. PUBLICATIONS 5

APPENDIX A. AN OPTICALLY BIASED LASER GYRO 6

APPENDIX B. BEAT-NOTE SENSITIVITY IN A ZEEMAN LASER GYRO: THEORY AND EXPERIMENT 16

APPENDIX C. MULTIOSCILLATOR LASER GYROS 19

APPENDIX D. A PROPOSED OPTICAL TEST OF PREFERRED FRAME COSMOLOGIES 37

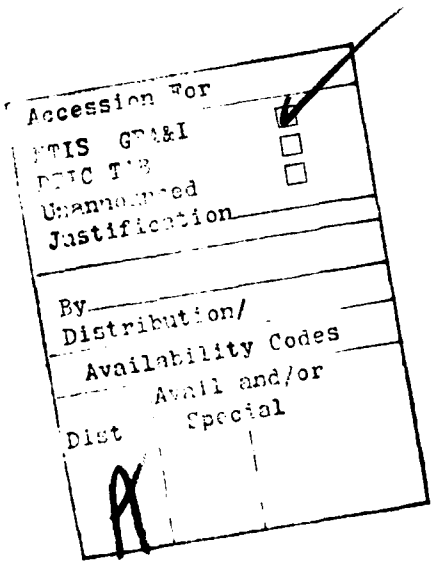

I. INTRODUCTION

Research on "Laser Gyro Theory Extension" was supported for the period from March 22, 1979, to September 22, 1980, by the Air Force Avionics Laboratory, Contract F33615-79-C-1744. Under this contract we have (a) tested the accuracy of our Zeeman laser gyro (ZLAG) theory by comparing its predictions with experimental results obtained at Litton, (b) investigated other multioscillator approaches to solving the lock-in problem, and (c) designed two earthbound experiments based on the Sagnac interferometer to test general and special relativity theories. We describe these investigations in this final report.

II. ZEEMAN LASER GYRO

We have been working with scientists at Litton Industries in the development of a Zeeman laser gyro (ZLAG). We have developed a vector laser theory that can handle polarized modes, inhomogeneously broadened media, atoms with some angular momentum and hyperfine structure, the presence of an applied magnetic field, and the presence of more than one isotope. This theory is based on semiclassical laser theory, and the resulting amplitude and frequency determining equations are solved for the case of the steady-state operation far from lock-in. The accuracy of this model was tested by comparing its predictions with experimental results obtained at Litton. This model was then used to perform the initial screening of possible ZLAG configurations. The goal is to find a ZLAG configuration that will give accurate rotation rate information under a wide range of operating conditions. The ZLAG beat note $\dot{\psi}$, for

example, is a function of detuning, Δ, and magnetic field on the active medium. Ideally, the beat note should be zero with no input rotation. However, nonlinearities in the active medium induce a null shift that varies with the magnetic field and detuning. Since an axial magnetic field is used for biasing the counterrotating modes and since cavity-length fluctuations that lead to detuning variations are unavoidable, we need to look for a ZLAG configuration that minimizes $|d\dot{\psi}/d\Delta|$.

In this study of the behavior of $|d\dot{\psi}/d\omega_{\omega}|$ for different values of magnetic field we were able to obtain the first significant correlation between theory and experiment for a ZLAG. We emphasize that the theoretical treatment does not involve any variable parameters and, in fact, the theoretical curves were generated before the experimental. From the view of using the ZLAG as a gyroscope, both theory and experiment predict a zero in $d\dot{\psi}/d\Delta$ for the configuration using a 35-MHz crystal and an 80-G axial magnetic field. Theory and experiment indicate that operation with, for example, a 440-MHz crystal is undesirable because there is no nonzero axial magnetic field that will make the gyro beat note insensitive to changes in cavity lengths. A Fortran IV version of the ZLAG computer program was delivered to Wright-Patterson Air Force Base. To our knowledge, this program is in operation in the PDP 11/03 computer in Dr. Kent Stowell's laboratory.

III. "2+2" GYRO

In the course of our ZLAG studies we discovered some interesting effects due to nonlinear interactions in a multimode ring laser. Our theory predicted that there are multioscillator ring lasers besides the ZLAG where

the locking problem may be overcome by nonmechanical means. These multi-oscillator gyros are characterized by two strong counterrotating modes and two weak counterrotating modes. A possible configuration is a ring cavity with a pair of strong axial modes and a pair of weak off-axial modes. Experiments using such a laser ("2+2" gyro) verified this prediction. Our gyro does not have a dead band. Also interesting is the appearance of a bias (reciprocal bias), which changes sign with a change in the direction of rotation. Preliminary theoretical investigations led us to believe that this bias may be based on the following features: (a) The nonlinear interaction between the active medium and the four gyro modes gives rise to relative phase angle terms that couple strongly the beat frequencies of the strong and weak modes. As a result the two beat frequencies are locked to each other. (b) Intensities between counterrotating modes vary with the beat note frequency. In the 2-mode gyro this variation introduces a reciprocal bias to the beat note; however, this bias is always less than the lock-in threshold. In the "2+2" gyro, experimental configurations exist in which the reciprocal bias is larger than the lock-in threshold. The construction of the "2+2" gyro is basically that of a two-mode gyro, except for the absence of a body dither. The laboratory device exhibits performance that is superior to that of a conventional laser gyro. Our attempts to understand the underlying "2+2" mechanism will, we hope, allow us to determine whether this performance is also realizable in a production model.

IV. APPLICATION OF LASER ROTATIONAL SENSORS TO PROBLEMS IN GENERAL AND SPECIAL RELATIVITY

In our on-going study involving the application of ring laser devices to problems in general and special relativity, we have designed two earth-bound experiments based on Sagnac interferometry. In these experiments, light from a laser is split into two beams and both beams are injected into a ring interferometer. One beam propagates in the clockwise direction in the interferometer and the other propagates in the counterclockwise direction. In the presence of rotation, a differential phase shift exists between the counterpropagating waves. By using nonlinear optical elements, we can translate this phase difference into a frequency difference that can be more precisely measured. We calculated the differential phase shift and the frequency difference in these experiments within the framework of parameterized post-Newtonian (PPN) formalism. PPN formalism is a theoretical framework to provide a comparison between various metric theories of gravitation. It is clear from our analysis that an earthbound experiment to observe the yet-unobserved geodetic procession and Lense-Thirring effect is within the reach of present technology.

V. PUBLICATIONS

The following papers have been published as a result of this contract support. Reprints are included as appendixes:

D. Z. Anderson, W. W. Chow, M. O. Scully and V. E. Sanders, "An optically biased laser gyro," Opt. Lett. 5(10):413-415, 1980.

V. E. Sanders, S. Madan, W. W. Chow, and M. O. Scully, "Beat-note sensitivity in a Zeeman laser gyro: theory and experiment," Opt. Lett. 5(3): 99-101, 1980.

W. W. Chow, J. B. Hambenne, T. J. Hutchings, V. E. Sanders, M. Sargent III, and M. O. Scully, "Multioscillator laser gyros," IEEE J. Quantum Electron. QE-16(9):918-935, 1980.

M. P. Haugan, M. O. Scully, and K. Just, "A proposed optical test of preferred frame cosmologies," Phys. Lett. 77A(1):88-90, 1980.

APPENDIX A

AN OPTICALLY BIASED LASER GYRO

Dana Z. Anderson, Weng W. Chow, and Marlan O. Scully†

Projektgruppe für Laserforschung
der Max-Planck-Gesellschaft
D-8046 Garching bei München

Department of Physics
Universities of New Mexico and Colorado
Albuquerque, New Mexico 87131 Boulder, Colorado 80209

and

Virgil E. Sanders*
Litton Guidance and Control Systems
Woodland Hills, California 91364

ABSTRACT

We describe a four-mode ring laser which exhibits none of the mode-locking characteristics which plague laser gyros. This laser is characterized by a bias which changes sign with a change in the direction of rotation and prevents the counter-propagating modes from locking. A theoretical analysis explaining the experimental results is outlined.

†Work supported by the Air Force Avionics Laboratory ASD, Contract #F33615-79-1744.

*Work supported by the U.S. Air Force Office of Scientific Research and the Air Force Avionics Laboratory ASD, Contract #33615-78-C-1524.

In this letter, we report the first observation of a "strapdown" ring laser which exhibits no frequency locking. It is well known that, for sufficiently high rotation rates, the beat note between the frequencies of the clockwise and anticlockwise traveling waves in a ring laser is proportional to the rotation rate of the device.[1] However, backscattering couples the counterrotating waves and at low rotation rates the frequencies tend to lock.[2] Laser gyros often contain body-shake dither mechanisms[3] to mitigate this lock-in problem. This method has similar mechanical support problems to the mechanical gyro. In addition, since a dithered gyro spends part of its time in the lock-in region, rotation information is sometimes lost. Purely optical methods[4] of circumventing the locking problem exist, for example, the Zeeman Laser Gyro.[5] These schemes often involve complicated setups and have the additional problem of polarization anisotropies.

In a number of recent papers,[6] another multioscillator approach to solving the locking problem was investigated. In these studies we considered pumping a traditional linearly-polarized ring laser hard enough so that two strong modes and two weak modes oscillated in the cavity (Fig. 1). A possible configuration is a ring laser with a pair of strong linearly-polarized axial modes and a pair of weak linearly-polarized off-axial modes. In a recent experiment using such a laser ("2+2" gyro), the lock-in region vanished altogether (Fig. 2) due to the occurrence of an induced bias much larger than the backscattering contributions. This bias (reciprocal bias) had the interesting feature of changing sign with a change in the direction of rotation. We will describe, in detail, our experiment and outline the theory which explains the vanishing lock-in and reciprocal-bias phenomena.

The experiment involved a 40 cm. equilateral triangle ring laser that was constructed from a solid block of CerVit. The laser was operated with a

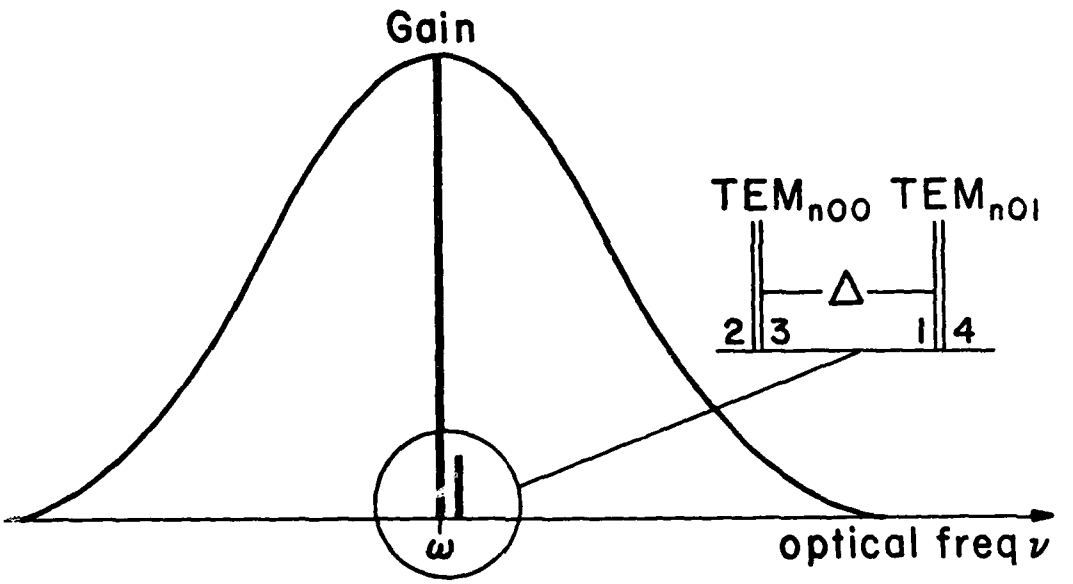

Fig. 1. Spectrum of "2+2" gyro. We have two strong modes, 2 and 3, and two weak modes, 1 and 4. Modes 1,2 are anticlockwise modes, while modes 3,4 are clockwise modes. Modes 1,4 and modes 2,3 belong to different transverse modes and are separated in frequency by $\Delta \simeq 60$ MHz. A scanning Fabry-Perot etalon was used to measure the frequency spectrum.

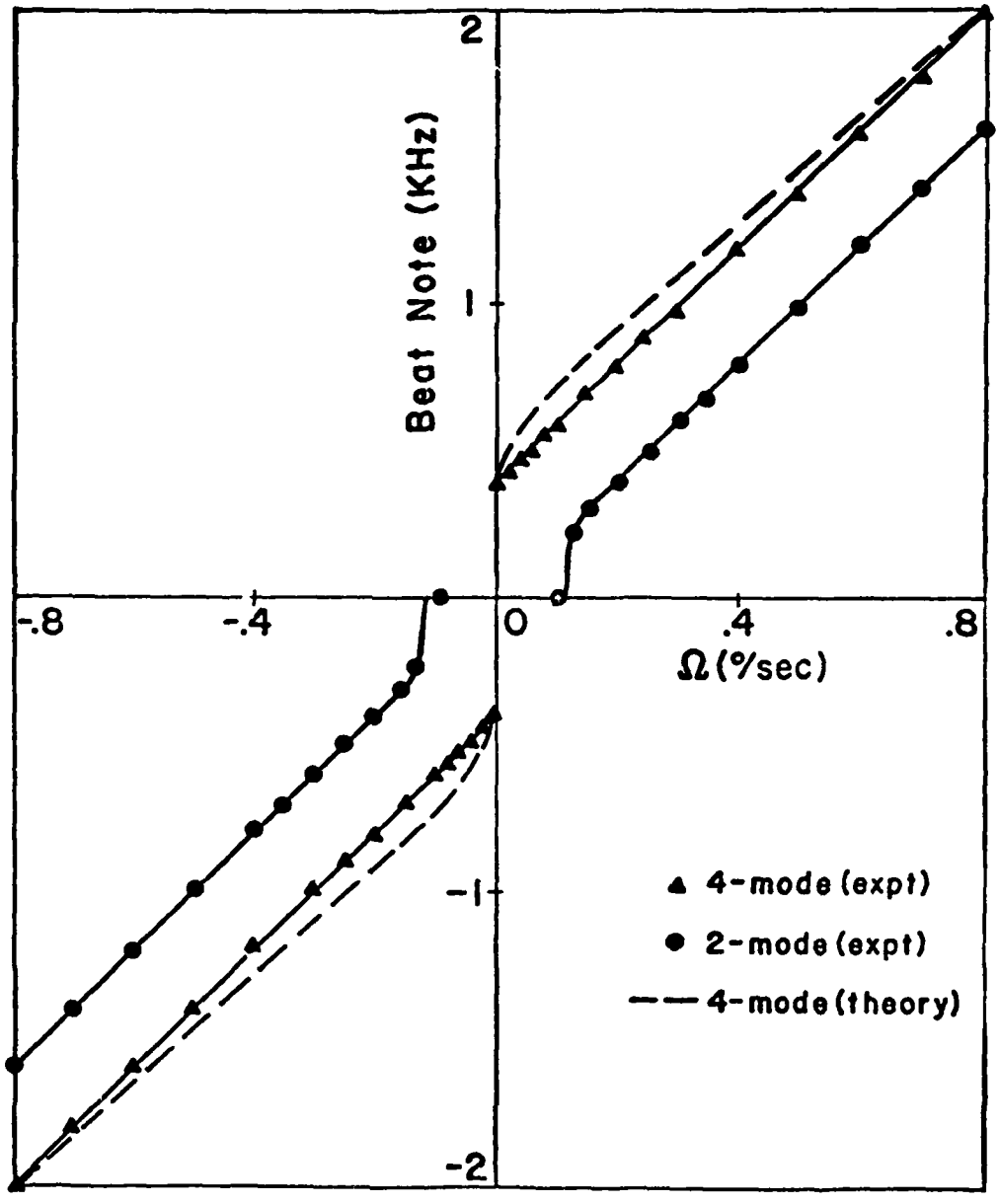

Fig. 2. Beat note vs. rotation rate for the "2+2" gyro. The points (▲) are the experimental results, while the dashed curve is obtained by solving Eq. (6). For comparison, we have included the beat note measured when the same laser was operated with only two modes. The actual two-mode curve contained a null shift of .75°/sec along the abscissa. We have removed this asymmetry which is probably due to Langmuir flow or frequency pulling and pushing.

2.4 to 3.5 Torr mixture of helium and neon (He:Ne ≈ 13:1). The neon contained equal amounts of ^{20}Ne and ^{22}Ne. A dual-anode and dual-cathode configuration was used to eliminate the effects of Langmuir[7] flow. Threshold currents for 2-mode operation ranged from 1.2 to 2.5 mA at gain center. To measure the beat note, we combined the counterrotating light beams with a prism and directed the resulting beam onto a detector whose output was fed into frequency counters. A piezo-electric crystal was attached to one of the mirrors so that we can change the cavity length and produce a detuning from the maximum of the gain curve, but this crystal was not servoed for cavity length control. This laser was also used in previous multioscillator experiments and further details are given in Ref. 6. The main modification was the removal of an intracavity aperture that was used to prevent the lasing of off-axis modes.

Four-mode (two TEM_{n00} and two TEM_{n01}) operation was achieved by increasing the plasma current and by adjusting the cavity length to obtain the proper detuning. The strong (TEM_{n00}) and weak (TEM_{n01}) mode spacing was approximately 60 MHz. Threshold for four-mode operation was roughly 3.5 times that for two mode. For our experiment, the strong to weak mode intensity ratio was typically 30:1, although similar results were obtained for ratios between 50:1 and 20:1. Fig. 2 shows a typical plot of beat note versus input rotation. Two striking features are the lack of a measurable dead band, and the discontinuity at approximately zero input rotation due to the reciprocal bias (the instantaneous rate accuracy for our experiment was .01°/sec). Also, the output exhibited no hysteresis and was linear with a scale factor of 2.4 KHz/(°/sec).

Other measurements were made to help us understand the underlying "2+2" mechanism. For instance, when all four light beams were compared we observed

only the frequency $(\nu_3 - \nu_2 + \nu_4 - \nu_1)/2$ which suggested that the beat notes $\nu_2 - \nu_2$ and $\nu_4 - \nu_1$ were equal. To check this, we measured the output of the clockwise and anticlockwise modes with different detectors. The clockwise signal was modulated at $\nu_4 - \nu_3$ and the anticlockwise signal was modulated at $\nu_1 - \nu_2$. Note that since TEM_{n00} was othogonal to TEM_{n01}, one must look at only a small portion of the beam to observe these modulations. When the output of the two photomultipliers were mixed, we observed no beat note which meant that $\nu_4 - \nu_3 = \nu_1 - \nu_2$ or $\nu_3 - \nu_2 = \nu_4 - \nu_1$. We also observed that each mode intensity was ac modulated. The modulation was basically sinusoidal with a frequency equal to the gyro beat note and an amplitude much less than the total mode intensity. The counterrotating mode intensities vary 180° out of phase with respect to each other.

A semiclassical laser theory of the "2+2" gyro yields electric field amplitude and frequency determining equations like Eqs. (25) and (26) in Ref. 5, but without the x-y anisotropy terms and with different values of the coefficients and ordering of the mode indices (nijk = 1234, 2134, 3412, 4321). In our analysis it is convenient to use the following variables:[8] (1) average strong-mode intensity, $I_s = (I_3 + I_2)/2$ and weak-mode intensity $I_w = (I_4 + I_1)/2$; (2) normalized intensity differences, $i_s = (I_3 - I_2)/2I_s$ and $I_w = (I_4 - I_1)/2I_w$. Simplifications to the equations may be made by noting that in the experiments the average intensities were constant and the ratios i_s and i_w were small. Furthermore, it was observed that the strong and weak mode beat notes were equal. Using the above information we find the working equations for our problem

$$\frac{di_s}{dt} = - 2\alpha_s i_s + 2b_s \sin\epsilon_s \cos\phi \qquad (1)$$

$$\frac{di_w}{dt} = - 2\alpha'_w i_w - 2\theta_{sw} I_s i_s - 2b_w \sin\epsilon_w \cos\phi \qquad (2)$$

$$\frac{d\phi}{dt} = S\Omega + \{b_s i_s \sin\varepsilon_s - b_w i_w \sin\varepsilon_w\} \sin\phi, \qquad (3)$$

where ϕ is the phase difference between the strong or the weak counterrotating modes, α is the net linear gain, b is the backscattering coefficient, ε is the backscattering angle, the subscripts s and w denote whether a quantity is associated with a strong or a weak mode, $\alpha_w' = \alpha_w - \theta_{sw} I_s$, θ_{sw} is the cross-saturation coefficient between the strong and weak modes, S is the scale factor, and Ω is the rotation rate. We have allowed for the strong and weak modes to have different backscattering coefficients and phases. In order to have constant total intensity, the backscattering angles ε_s and ε_w have to be old multiples of $\pi/2$. Since the strong modes are far above threshold, $\alpha_s >> \dot{\phi}$, and in the case of the weak modes, it is possible that $\alpha_w' << \dot{\phi}$. In this limit,

$$i_s = b_s \sin\varepsilon_s \cos\phi/\alpha_s \qquad (4)$$

and

$$i_w = -2Ab_w \sin\varepsilon_w \sin\phi/\dot{\phi}\ , \qquad (5)$$

where $A = 1 + \theta_{sw} b_s \sin\varepsilon_s/[(\beta_s - \theta_s) b_w \sin\varepsilon_w]$. By substituting Eqs. (4) and (5) into Eq. (3), we obtain an expression for the "2+2" beat note

$$\dot{\phi} = S\Omega + Ab_w^2/\dot{\phi} - A(b_w^2/\dot{\phi}) \cos 2\phi + b_s^2/(2\alpha_s) \sin 2\phi. \qquad (6)$$

Note that in the absence of the weak modes, Eq. (6) reduces to the usual lock-in equation where the lock-in threshold is $|S\Omega| = b_s^2/(2\alpha_s)$. To determine the effect of the weak modes we solve Eq. (6) for $\dot{\phi}$. For the purpose of discussion, we neglect the last term. This is justified because the bias obtained is much greater than $b_s^2/(2\alpha_s)$. By doing so we have a quadratic equation in $\dot{\phi}$, with the solution

$$\dot{\phi} = S\Omega/2 \pm \sqrt{(S\Omega/2)^2 + 2b_w^2 A \sin^2\phi} \quad , \tag{7}$$

where the plus sign is for positive rotation and the negative sign is for negative rotation. As the rotation rate approaches zero from the positive side, we have

$$\dot{\phi} = \sqrt{2A}\, b_w |\sin\phi| \tag{8}$$

We see here that the stationary values ($\dot{\phi} = 0$) $\phi = 2n\pi$ are unstable, and therefore that no lock-in band is encountered. Phase fluctuations due to for example mechanical vibrations kick the system for $\phi = 2n\pi$ points toward $\phi = 2(n+1)\pi$, but not in the reverse direction. Since Eq. (8) shows that the phase can only increase, we obtain a positive bias which may be as big as $\sqrt{2A}\, b_w$. Similarly as we approach zero input rotation from the negative side, a negative bias equal in magnitude to the positive bias is encountered.

At this point one may question whether it is really necessary to have four modes. It would seem from our derivation that as long as the excitation is sufficiently low such that $\alpha << \dot{\phi}$, an induced bias and a zero lock-in band can be obtained. A closer examination shows that in the two-mode case the assumption $\alpha << \dot{\phi}$ implies that the two mode amplitudes differ significantly and in an unstable fashion which eventually lead to one of the intensities being close to zero. In the four-mode case, the term $\theta_{sw} I_s$ in Eq. (2) causes $i_w \simeq \sqrt{A}$ at zero input rotation. So by making a proper choice of backscattering angles, i.e., $\sin\varepsilon_s = -\sin\varepsilon_w$, i_w may be made to remain small.

To determine the reciprocal bias, Eq. (7) was solved numerically with a computer. The two-mode backscattering contribution was included by replacing $S\Omega$ with $S\Omega + b_s^2/(2\alpha_s) \sin 2\phi$ and a rapidly varying function F(t) was added to ϕ to account for the presence of noise. This function F(t) has a zero

time average and a 5 Hz amplitude, which is the uncertainty of the measured beat note. The two-mode lock-in coefficient is measured to be around 250 Hz and this in turn gives $b_w \simeq 10$ KHz. We estimated the intensity variation $i_w \simeq 20\%$, giving A = .04. Finally, since we have a 40 cm cavity, S = 2 KHz/(°/sec). The theoretical curve corresponding to these values is shown in Fig. 2(dashed lines). Thus we conclude that a careful analysis of the four-mode "2+2" problem provides us with a satisfactory explanation of the observed bias and reduced lock-in. A more complete theoretical analysis will be published elsewhere.

In conclusion, we have constructed a four-mode linearly-polarized ring laser which had no lock-in region. The beat note exhibited no hysteresis and was essentially a linear function of input rotation. Preliminary theoretical investigations lead us to believe that the zero lock-in region may be based on the following features.

1. The nonlinear interaction between the active medium and the four gyro modes gives rise to relative phase angle terms which lock the beat frequencies of the strong and weak modes.

2. The mode intensities vary with the beat frequency. In the two-mode gyro this variation introduces a bias which is always less than the lock-in threshold. In the four-mode case there exists experimental configurations where the induced bias is larger than the lock-in threshold.

Further investigations are being carried out, particularly, in determining the dependence of the gyro on frequency detuning, and on the strong and weak mode intensities. Finally, we wish to emphasize that the construction of the "2+2" gyro is basically that of a two-mode gyro except for the absence of a body dither and an intracavity aperture. Therefore, with minor changes in the present production gyro one may be able to

vastly improve its performance. Whether this is realizable depends on our understanding of the underlying mechanism.

We wish to thank Prof. Murray Sargent III for helpful discussions.

REFERENCES

1. A. H. Rosenthal, J. Opt. Soc. Am. 52, 1143 (1962); W. M. Macek and D. T. M. Davis, Jr., Appl. Phys. Lett 2, 67 (1963); F. Aronowitz, Phys. Rev. A 139, 635 (1965); E. J. Post, Rev. Mod. Phys. 39, 475 (1967); T. H. Hutchings, J. Winocur, R. H. Durrett, E. D. Jacobs, and W. L. Zingery, Phys. Rev. 152, 467 (1966); C. Whitney, Phys. Rev. 181, 535 (1969).
2. F. Aronowitz and R. J. Collins, J. Appl. Phys. 44, 130 (1970); Appl. Phys. Lett. 9, 55 (1966).
3. F. Aronowitz, "The Laser Gyro," in Laser Applications, M. Ross, Ed. (Academic, New York, 1971), pp. 131-200.
4. G. Yntema, D. Grant, Jr. and R. Warner, U. S. Patent 3,862,803, Jan. 28, 1975; K. Andringa, U. S. Patent 3,741,657, June 26, 1973.
5. W. W. Chow, J. B. Hambenne, T. J. Hutchings, V. E. Sanders, M. Sargent III and M. O. Scully, (to be published in IEEE J. Quantum Electronics).
6. M. O. Scully, V. Sanders and M. Sargent III, Opt. Lett. 3, 43 (1978); V. Sanders, D. Anderson and M. O. Scully, Proc. SPIE 22nd Symp. on Laser Inertial Rotation Systems (1978); D. Anderson, W. W. Chow, V. Sanders and M. O. Scully, App. Optics 18, 941 (1979).
7. I. Langmuir, J. Franklin Inst. 196, 751 (1923).
8. F. Aronowitz and W. L. Lim, IEEE J. Quantum Electronics QE-13, 388 (1977).

APPENDIX B

Beat-note sensitivity in a Zeeman laser gyro: theory and experiment

Virgil E. Sanders and Shobna Madan

Litton Guidance and Control Systems, Woodland Hills, California 91364

Weng W. Chow and Marlan O. Scully

Optical Sciences Center and Department of Physics, University of Arizona, Tucson, Arizona 85721

Received October 30, 1979

We present data that are the first significant correlation between theory and experiment of a Zeeman laser gyro. This study concerns the behavior of the Zeeman laser-gyro beat note as a function of detuning, magnetic field, and optical activity bias. Both experiment and theory indicate the presence of a gyro configuration that is insensitive to cavity-length changes. This result has obvious importance and relevance to practical laser-gyro devices.

The fundamental principle underlying laser-gyroscope operation involves the observation that a rotating optical ring resonator has two different round-trip path lengths.[1] This translates into a frequency difference between the counterrotating modes in the gyro. Owing to the scattering of energy from one mode into the other, the beat frequency "locks" (i.e., vanishes) for small-input rotation rates.[2] Since technological constraints prevent the elimination of this dead band, laser gyros are often mechanically dithered to reduce the effects of lock-in.[3] Although dithered gyros are suitable in both size and sensitivity for aerospace guidance applications,[4] the potential of laser gyros is not fully realized until one has an instrument that contains no moving mechanical components. Because of this, multioscillators[5] became interesting as candidates for the next generation of laser gyros.

A class of multioscillator gyros, the Zeeman laser gyro (ZLAG),[6-9] consists of two two-mode ring lasers sharing the same cavity and distinguished from each other by their electric-field polarization (Fig. 1). A fixed bias is introduced into the cavity to circumvent the problems of lock-in, i.e., the left- and right-handed gyros have the beat frequencies

$$\nu_2 - \nu_3 = -S\Omega + \text{bias} \tag{1}$$

and

$$\nu_4 - \nu_1 = S\Omega + \text{bias}, \tag{2}$$

respectively, where S is the scale factor and Ω is the input rotation rate. Rotation-rate information is obtained by taking the difference of the beat notes from the two coresident ring lasers,

$$\dot{\psi} \equiv \nu_4 - \nu_1 - \nu_2 + \nu_3 = 2S\Omega. \tag{3}$$

We see that the bias cancels so gyro accuracy is no longer hampered by bias instabilities and, in addition, twice the rotation-rate sensitivity results.

There remains the question of how accurately one can determine input rotations. The ZLAG beat note, for example, is a function of detuning, Δ, and magnetic field, H, on the active medium. Ideally the beat note should be zero with no input rotation. However, nonlinearities in the active medium induce a null shift, which varies with the magnetic field and detuning. Since an axial magnetic field is used for biasing the counterrotating modes and since cavity-length fluctuations that lead to detuning variations are unavoidable, we need to look for a ZLAG configuration that minimizes $|d\dot{\psi}/d\Delta|$.

In this Letter, we describe the experimental and theoretical studies on the ZLAG beat note, $\dot{\psi}$, at zero-input rotation as a function of axial magnetic field and detuning. Besides the practical aspect of finding a gyro configuration that is insensitive to detuning and magnetic-field fluctuations, the data presented in this Letter are significant for two additional reasons: (1) The ZLAG can only be treated by a vector theory,[10,11] i.e., the electric-field polarizations and the magnetic sublevels of the atoms have to be taken into account. Our studies provide a test for the ZLAG theory that is the most general and comprehensive (and, therefore, the most complicated) Lamb-theory extension to date. (2) The precision of measurements involving differences

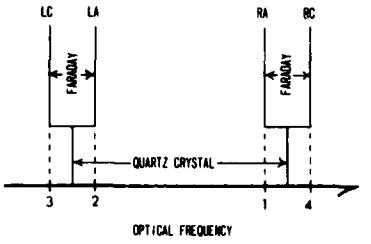

Fig. 1. Optical spectrum of a Zeeman laser gyro. L(R) indicates left (right) circular polarization; A(C) indicates anticlockwise (clockwise) mode.

Reprinted from Optics Letters, Vol. 5, page 99, March, 1980

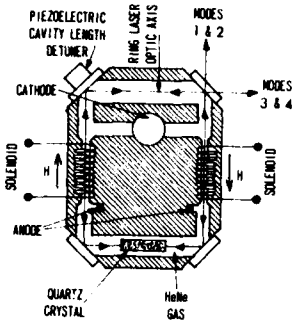

Fig. 2. Experimental apparatus for a Zeeman laser gyro.

in frequencies (beat notes) is that associated with quantum noise limit of the laser linewidth (typically 10^{-3} Hz). For laser frequencies of 10^{14} Hz, this resolution is one part in 10^{17}. Measurements of absolute frequency of the individual modes, intensities, and polarization characteristics do not compare in precision to this measurement.

The He–Ne ring laser used in this study (see Fig. 2) was constructed from a solid block of CerVit. Clearance holes, gain bores, and an aperture were machined into this block to accommodate both the optical and electrical discharge paths. Both mirrors and electrodes were affixed to polished surfaces on the block. The ring cavity has two separate, equal gain regions. Each of the gain regions has a magnetic coil surrounding only the full gain bore regions of the cavity. These coils provide the Faraday bias. The Faraday bias is linearly related to the magnitude of the magnetic field (about 2 kHz per gauss). Modes of different polarizations are separated in frequency by an optically active quartz crystal oriented with its optic axis parallel to the laser beam. The frequency splitting from the quartz crystal was approximately 35 MHz for one of the cases presented in the Letter and 440 MHz for the other.

Semiclassical laser theory involves solving self-consistently the coupled Maxwell and Schrödinger equations.[12] The procedure for obtaining the frequency- and amplitude-determining equations for the four electric-field modes is first to calculate, through the Schrödinger equation to third order in the interaction potential, the dipole moment induced in each atom of the active medium. By statistically summing the individual atomic dipoles, one obtains an expression for the polarizibility. This expression for the polarizibility is then used in the field equation. The field equation, which is obtained from Maxwell's equations, may be separated into four equations for the time development of the electric-field amplitudes and four equations for the frequencies. These equations are coupled by terms containing the relative phases of the electric field. Since we are at present only interested in the behavior of the ZLAG outside of the lock-in region, these terms tend to average to zero. This decouples the amplitude equations from the frequency equations. In addition, we are interested only in the cases in which the electric-field amplitudes are at steady state and the four modes are above threshold. We found, by looking at the various coupling parameters, that under certain conditions the field modes are weakly coupled.[13] In these cases, the problem reduces to solving the four algebraic amplitude equations simultaneously for the stable solutions. These equations are

$$\alpha_n - \sum_{m=1}^{4} \theta_{nm} I_m = 0, \tag{4}$$

where $n = 1, 2, 3, 4$; α_n is the nth-mode net gain; θ_{nm} is the saturation coefficient between modes n and m; and I_m is the mth-mode intensity. The values for the amplitudes obtained are then used in the frequency equations

$$\nu_n + \dot{\phi}_n = \Omega_n + \sigma_n - \sum_{m=1}^{4} \tau_{nm} I_m \tag{5}$$

to determine the lasing frequencies. For Eq. (5), $\nu_n + \dot{\phi}_n$ is the nth-mode lasing frequency, Ω_n is the nth-mode

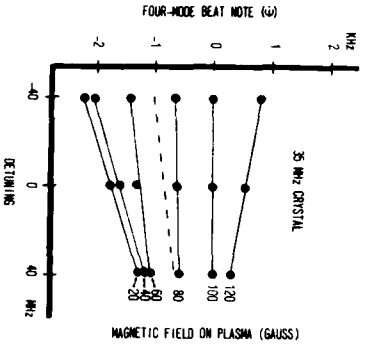

Fig. 3. Four-mode beat note versus detuning for different values of axial magnetic fields. The values of the axial magnetic field are shown on the right vertical axis. This gyro has a 35-MHz quartz crystal in the cavity. These data were obtained with zero-input rotation. Note that at 80 G the slope of the curve is approximately zero. The dash curve is the theoretical result for $H = 80$ G.

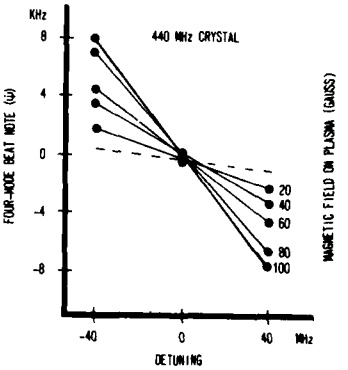

Fig. 4. Four-mode beat note versus detuning for different values of axial magnetic fields. This gyro has a 440-MHz quartz crystal in the cavity. These data were obtained with zero-input rotation. The dash curve is the theoretical result for $H = 20$ G.

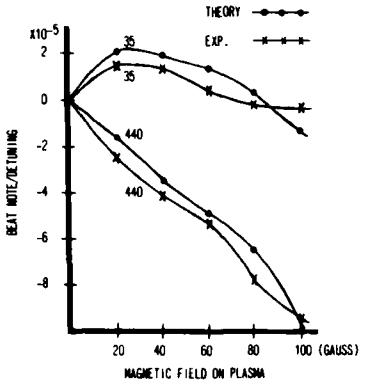

Fig. 5. Derivative of the beat note with respect to detuning versus magnetic field for quartz crystals of 35 and 440 MHz. The experimental values are obtained from Figs. 3 and 4. The theoretical values are the result of a numerical analysis based on the Zeeman laser-gyro theory.

passive cavity frequency, σ_n is the nth-mode frequency-pulling term, and τ_{nm} is the mode-pushing coefficient between modes n and m.

To summarize, the features of our theory are as follows: the cavity has four circularly polarized modes, the medium is inhomogeneously broadened with atoms of some given angular momenta, and it is possible to have more than one isotope and for it to be in an applied magnetic field. Details of the ZLAG theory are presented in Refs. 11 and 13.

The data shown in Fig. 3 are associated with the 35-MHz crystal. The vertical scale represents the four-mode laser-gyro beat note, $\dot{\psi}$. This beat note is detected from the electrical output of a photodiode, i.e., the four beams (two from each direction around the ring) are spatially aligned coaxially with mirrors and beam splitter and directed to the surface of the photodiode heterodyne receiver. Detuning is the difference between the mean optical frequency of all four modes and the midway point between the natural 6328-Å transitions of ^{20}Ne and ^{22}Ne of the He–Ne gain media. These transitions are approximately 875 MHz apart. Detuning of the optical frequency is affected by changing the cavity length (see Fig. 2). The magnetic-field strength on the gas plasma is indicated to the right of each curve. Also shown is the theoretical curve for $H = 80$ G. Both theory and experiment are in good agreement, and they both indicate a linear relationship between $\dot{\psi}$ and detuning. There is also good agreement between experiment and theory for the other values of H. Figure 4 is similar to Fig. 3 except that the data in Fig. 4 are associated with the 440-MHz crystal. Figure 5 is a summary of the theoretical and experimental data for all values of the magnetic field. The vertical scale is the derivative of the four-mode beat note with respect to detuning, and the horizontal scale represents the magnetic-field strength on the gas plasma.

In conclusion, we present data that we believe to be the first significant correlation between theory and experiment for a ZLAG. We emphasize that the theoretical treatment does not involve any variable parameters. In fact, the theoretical curves were generated before the experimental. From the point of view of using the ZLAG as a gyroscope, it is interesting to note that both theory and experiment predict a zero in $d\dot{\psi}/d\Delta$ for the configuration using a 35-MHz crystal and an 80-G axial magnetic field. Theory and experiment indicate that operation with, for example, a 440-MHz crystal is undesirable because there is no nonzero axial magnetic field that will make the gyro beat note insensitive to changes in cavity length.

The research of V. E. Sanders was supported by the U.S. Air Force Office of Scientific Research and the Air Force Avionics Laboratory ASD under contract 33615-78-C-1524; that of W. W. Chow and M. O. Scully, by the Air Force Avionics Laboratory ASD under contract F 33615-79-C-1744.

References

1. C. V. Heer, Bull. Am. Phys. Soc. **6**, 58 (1961); E. J. Post, Rev. Mod. Phys. **39**, 475 (1967).
2. F. Aronowitz and R. J. Collins, Appl. Phys. Lett. **9**, 55 (1966).
3. J. Killpatrick, IEEE Spectrum **4**, 44 (1967).
4. F. Arnowitz, Proc. Soc. Photo-Opt. Instrum. Eng. **157**, 2 (1978).
5. H. deLang, Philips Res. Rep. **19**, 439, (1964).
6. This idea of using two coresident two-mode gyros and obtaining the input rotation rate by measuring the difference in the two beat notes originated in the differential laser gyro (DILAG) (Refs. 7 and 8). Stated in the patents for the DILAG is the use of a Faraday crystal as a bias element. We use the term Zeeman laser gyro (ZLAG) to describe a laser gyro that uses the DILAG method of measuring rotation rates, and an axial magnetic field applied on the active medium for the bias.
7. G. Yntema, D. Grant, Jr., and R. Warner, U.S. Patent 3,862,803, January 28, 1975.
8. K. Andringa, U.S. Patent 3,741,657, June 26, 1973.
9. V. Sanders, S. Madan, W. Chow, and M. Scully, in *Proceedings of National Aerospace and Electronics Conference* (Institute of Electrical and Electronics Engineers, New York, 1979), Vol. 1, p. 2.
10. C. V. Heer and R. D. Graft, Phys. Rev. **140A**, 1088 (1965).
11. D. Hanson and M. Sargent III, Phys. Rev. A **9**, 466 (1974).
12. W. E. Lamb, Jr., Phys. Rev. **134**, A 1429 (1964); L. N. Mengozzi and W. E. Lamb, Jr., Phys. Rev. A **8**, 2103 (1973).
13. W. Chow, J. Hambeene, M. Sargent III, and M. Scully, IEEE J. Quantum Electron. **QE-15**, 1301 (1979).

Papers

APPENDIX C

Multioscillator Laser Gyros

WENG W. CHOW, JAREL B. HAMBENNE, THOMAS J. HUTCHINGS, VIRGIL E. SANDERS, MURRAY SARGENT III, AND MARLAN O. SCULLY

(Invited Paper)

Abstract—The two-mode ring laser gyro is reviewed. Standard bias and dither techniques are discussed that alleviate the mode locking encountered at low rotation rates. The four-mode DILAG (differential laser gyro) and its magnetic field extension the ZLAG (Zeeman laser gyro) are defined and analyzed. These devices contain two coresident ring lasers of opposite helicity and may have no moving parts. The mode-locking problems are overcome with the use of various biases that cancel out in the rate signal. A semiclassical analysis is reviewed that gives the electric field amplitudes and frequencies of the four modes in the presence of multilevel atoms, cavity anisotropy, and backscattering. It is shown that without mode-locking contributions, laser operation can be approximated very well by four independently oscillating modes. The Zeeman effects are considered. Novel scalar four-mode schemes are also discussed that circumvent the mode-locking problem.

I. Introduction

SINCE its conception [1]-[3] and first demonstrated application [4] in the early 1960's, the ring laser gyroscope has been brought to an advanced stage of instrumental development. Recent disclosures [5], [6] reveal gyros that are suitable in both size and sensitivity for aerospace guidance applications. Typical aircraft inertial navigation systems require instruments capable of sensing rotation rates near 0.01°/h. Present ring laser gyros are capable of sensing rotation rates down to 0.001°/h (0.0001 earthrate). Compared to its mechanical counterpart, the laser gyro is substantially cheaper, lighter, has no start-up time, and is a "strapped-down" device. Furthermore, its lifetime has been extended to several tens of thousands hours.

A basic two-mode ring laser gyroscope has two independent counterrotating waves oscillating in an optical ring cavity (see Fig. 1). The frequencies of the waves depend linearly on the rotation rate of the cavity with respect to an inertial frame [7], [8]. Consequently, the rotation rate is proportional to the beat note. Ideally the ring gyro contains no moving parts. In practice, however, the two-mode laser gyro often must be mechanically dithered [9]-[11] to keep the counterrotating traveling waves from locking at low rotation rates [12], [13]. Investigations [14], [15] show that the lock-in problem can be alleviated by using a ring cavity that contains more than one pair of counterrotating modes. With these so-called multioscillators in mind, we may indeed hope to have a gyroscope with no moving parts.

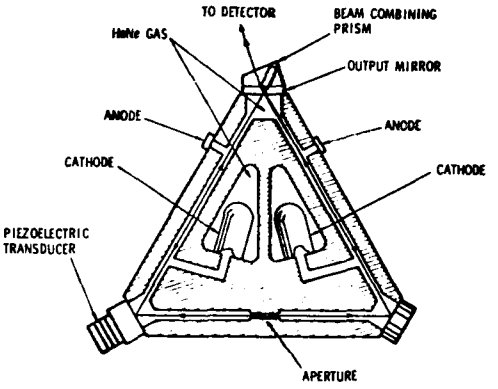

Fig. 1. A basic two-mode ring laser gyro. The two counterrotating waves are combined by a prism and the beat note gives the rotation rate about an axis normal to the plane of the ring cavity.

This paper concentrates on the use of four-mode multioscillators as laser gyros. For completeness we begin by giving an overview of the fundamental principles underlying two-mode laser gyro operation and the problems encountered in rotation rate measurements with laser gyros (Section II). The remaining sections are devoted to multioscillator concepts. In Section III, the most developed of the multioscillator laser gyros, the ZLAG-Zeeman laser gyro, is described. This device is an

Manuscript received December 5, 1979; revised May 5, 1980. The work performed by V. E. Sanders was supported by the U.S. Air Force Office of Scientific Research and the Air Force Avionics Laboratory ASD under Contract 33615-78-C-1524. The work performed by M. O. Scully was supported by the Air Force Avionics Laboratory under Contract F 33615-79-C-1744.

W. W. Chow, J. B. Hambenne, and M. Sargent III are with the Optical Sciences Center, University of Arizona, Tucson, AZ 85721.

T. J. Hutchings and V. Sanders are with Litton Industries, Woodland Hills, CA 91364.

M. O. Scully was with the Optical Sciences Center, University of Arizona, Tucson, AZ 85721. He is now with the Department of Physics, University of New Mexico, Albuquerque, NM 87106.

0018-9197/80/0900-0918$00.75

extension of the earlier DILAG-differential laser gyro [14], [15]. Both contain two pairs of two counterrotating waves, each pair characterized by one orthogonal circular polarization. The rotation rate is given by the difference between the two gyro beat frequencies such that the biases used cancel out. The DILAG depends on many parameters, e.g., excitation current, isotopic abundances, cavity length, optical activity, and Faraday bias. The ZLAG is a DILAG with a magnetic field applied to the laser medium itself. This approach yields a Faraday bias without the use of a quartz crystal, allowing operation with no intracavity optical elements. Since fabrication difficulties require one to be selective in the experimental configurations studied, there is a need for a theoretical model to perform the initial screening. A ZLAG model based on the Zeeman ring laser theory [16]-[18] is described in Section IV. The equations describing the ZLAG simplify under certain operating conditions as shown in Section V. Section VI gives details of ZLAG construction and compares theoretical predictions with experimental observations. Finally, Section VII discusses an alternative optical approach to solving the locking problem in which we hope to replace the mechanical dither used in two-mode gyros by a variation of the multioscillator principle involving a combination of two weak and two strong optical modes in a scalar field ring cavity.

In Appendix I, the eight amplitude and frequency determining equations for the ZLAG are written explicitly. Appendix II contains a description of the Yntema diagrams which simplify the translation between mode frequencies and atomic velocities. These diagrams developed by Yntema appear here for the first time in the literature.

II. Laser Gyro Operation

A. Principle of Operation

The fundamental principle underlying laser gyroscope operation involves the observation that a rotating optical ring resonator has two different roundtrip path lengths [7], [8]. For the slow rotation rates encountered in gyro applications, this path length effect may be treated nonrelativistically. From Fig. 2, the path lengths for clockwise and anticlockwise modes are

$$L_c = 2\pi R + \Omega R \tau_c \tag{1}$$

$$L_a = 2\pi R - \Omega R \tau_a \tag{2}$$

respectively, where the rotation rate Ω is positive for clockwise rotations. The second term on the right-hand side (RHS) of (1) is the extra distance the clockwise wave has to travel because the starting point has moved a distance $\Omega R \tau_c$ in the time the clockwise wave takes to complete a roundtrip (τ_c). Similarly, $\Omega R \tau_a$ is the distance the starting point has moved, in the opposite direction, in the time it takes the anticlockwise wave to complete its roundtrip (τ_a). Noting that $\tau_c = L_c/c$ and $\tau_a = L_a/c$, we find the path difference

$$\Delta L = L_c - L_a = 4\pi R \frac{\Omega R}{c}. \tag{3}$$

Since the mode frequencies in a ring laser have to satisfy a periodic boundary condition, the difference in path lengths

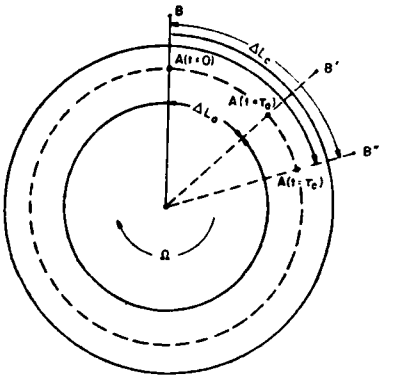

Fig. 2. A simplified Sagnac configuration. If two runners started running in opposite directions on a clockwise rotating disk when point A, which is fixed on the disk, coincides with point B in the laboratory (fixed reference frame), then by the time, τ_a, the anticlockwise runner reached A again, A would have moved to B' in the laboratory. Similarly, when the clockwise runner completes his roundtrip at time τ_c, point A would be in position B'' in the laboratory frame. Hence, the actual distances traveled by both runners are different.

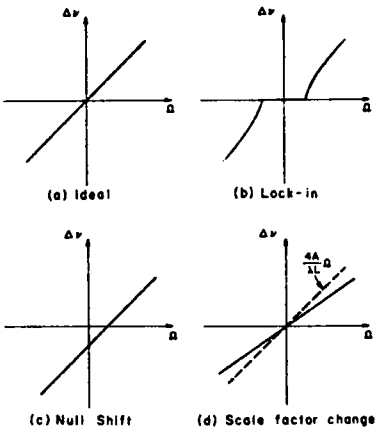

Fig. 3. Sources of error in a laser gyro.

corresponds to a frequency difference between the counterrotating modes, i.e., $\Delta\nu/\nu = -\Delta L/L$, where ν is the approximate cavity frequency and L is the cavity length. Combining this with the path difference [see (3)], we find the beat note

$$\Delta\nu = S\Omega = 8\pi A/(\lambda L)\Omega \tag{4}$$

where S is the scale factor, A is the area enclosed by the ring, and $\lambda = 2\pi c/\nu$ is the laser wavelength. For example, a 40 cm ring cavity, operating at the He-Ne transition of 6328 Å, when rotated at a rate of 10°/h, gives a beat frequency of 6 Hz which is measurable using heterodyne techniques.

B. Error Sources

According to (4), a graph of the rotation rate versus the beat frequency is a straight line passing through the origin [see Fig. 3(a)]. Three kinds of errors cause the gyro to deviate from this ideal straight line. First, due to backscattering [12], localized losses [13], and polarization anisotropies [19], [20], the mode frequencies lock at low rotation rates [see Fig. 3(b)]. This

results in a zero beatnote for a nonzero rotation. Two other kinds of error are fluctuations in the null shift [see Fig. 3(c)] and scale factor [see Fig. 3(d)], which affect the accuracy of rotation-rate measurements even when the gyro is operating far from the lock-in region. Null shifts are caused by noise in the bias used to eliminate lock-in, Fresnel drag [21], differences in isotopic abundance, or frequency pulling and pushing effects. Variations in the scale factor can be caused by mode pulling and pushing effects.

C. Active Medium

The design of a two-mode laser gyro consists of selecting a gain medium and cavity configuration that minimize pushing and pulling errors, and of choosing a biasing scheme to reduce the locking effect. The choice of helium and an equal mixture of two isotopes of neon (Ne^{20} and Ne^{22}) [21], [22] was made in 1967 and remains the best to date. Both theoretical [23], [24] and experimental [25] laser linewidth values for the He-Ne laser have a resolution better than 1 Hz in 1 s. This resolution improves as the inverse square root of the measurement time. With state of the art low loss mirrors, this gas mixture requires considerably less than a 10 cm gain medium to sustain laser oscillation at 6328 Å and thus satisfies the requirements for a small gyro. Spatial hole-burning competition effects in homogeneously broadened media such as ion gasses, solid state, and dye ring lasers typically result in unidirectional operation, rendering these media useless for gyro operation. Spectral hole-burning leads to strong mode competition near line center in single-isotope inhomogeneously broadened gain media. This competition is nearly negligible in the dual isotope inhomogeneously broadened medium [21], [22], [26]. With the lasing frequency roughly midway between the Ne^{20}/Ne^{22} natural transition frequencies, the mode pushing and pulling effects are tolerable.

D. Biasing Techniques

Lock-in typically occurs at rotation rates of around 0.1°/s. A biasing scheme is required to overcome this problem. The first biasing schemes suggested were those providing a constant effective rotation rate which is larger than the largest rate to be measured. The most popular of these schemes uses the nonreciprocal Faraday effect [29], [30], [21], [9]. Application of an axial magnetic field to an amorphous, isotropic material placed in the ring cavity splits the cavity frequencies of the two counterrotating laser modes. The beat note is proportional to the product of the magnetic field and the material length. The constant of proportionality is the Verdet constant of the material. This scheme was not fruitful for two reasons: 1) the element was sensitive to stray magnetic fields; 2) the suitable materials with large Verdet constants have large thermal expansion. The changes in size with temperature makes it difficult to fix the Faraday element in the cavity.

Another scheme providing a constant beat note offset uses the Fresnel-Fizeau effect. This effect, like the Faraday effect, is optically nonreciprocal and is due to a transparent dielectric medium moving with a constant velocity along the axis of the laser cavity. The induced beat note is given by

$$\Delta\nu = 2(n^2 - 1)\, vl/\lambda L \tag{5}$$

where n is the refractive index of the dielectric, v is its velocity, l is the dielectric length, λ is laser wavelength, and L is the total optical cavity length. Both a flowing fluid [29] and a spinning glass wheel [31] have been used. As with the Faraday cell, maintaining a constant bias to within 0.01°/h is mechanically difficult.

The stability problems associated with constant biasing techniques are eliminated by alternating the bias in time (dither) [9]. This occurs since over each cycle the bias averages to zero and one is left with just the input rotation. To see this we note that the instantaneous beat note for an undithered system is given by [12]

$$\dot{\psi} = a + b \sin \psi \tag{6}$$

where $\dot{\psi}$ is the beat note, a is the frequency difference due to rotation, mode pulling, and pushing effects, and b is the backscattering coefficient. If a is greater than b, $\dot{\psi}$ is never zero. However, if a is less than or equal to b in magnitude, $\sin \psi$ eventually assumes a value such that $\dot{\psi} = 0$. In this case ψ does not change and the beat note remains at zero, i.e., the frequencies are locked. The beat note for a dithered system is given by [10]

$$\dot{\psi} = a + b \sin \psi + c \cos(\omega_d t) \tag{7}$$

where c and ω_d are the amplitude and frequency of the oscillating bias. The bias amplitude c is made large so that the gyro is unlocked most of the time. To a good approximation

$$\psi(t) \simeq at + \frac{c}{\omega_d} \sin(\omega_d t). \tag{8}$$

Substituting (8) back into (7) we find

$$\dot{\psi} \cong a + b \sin\left(at + \frac{c}{\omega_d} \sin \omega_d t\right) + c \cos \omega_d t. \tag{9}$$

Using

$$\cos\left(\frac{c}{\omega_d} \sin \omega_d t\right) = J_0\left(\frac{c}{\omega_d}\right) + 2 \sum_{n=1}^{\infty} J_{2n}\left(\frac{c}{\omega_d}\right) \cos(2n\omega_d t)$$

and

$$\sin\left(\frac{c}{\omega_d} \sin \omega_d t\right) = 2 \sum_{n=1}^{\infty} J_{2n-1}\left(\frac{c}{\omega_d}\right) \sin[(2n-1)\omega_d t] \tag{10}$$

we write (10) as

$$\dot{\psi} = a + b \sin at \left\{ J_0\left(\frac{c}{\omega_d}\right) + 2 \sum_{n=1}^{\infty} J_{2n}\left(\frac{c}{\omega_d}\right) \cos(2n\omega_d t) \right\} + b \cos at \left\{ 2 \sum_{n=1}^{\infty} J_{2n-1}\left(\frac{c}{\omega_d}\right) \sin[(2n-1)\omega_d t] \right\} + c \cos \omega_d t. \tag{11}$$

Since the gyro measurement time is greater than a dither period, (11) reduces to

$$\dot{\psi} = a + bJ_0\left(\frac{c}{\omega_d}\right) \sin at. \tag{12}$$

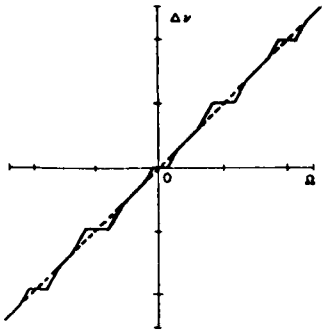

Fig. 4. The demodulated beat note versus rotation rate for a sine-wave dithered gyro. The dashed line shows ideal gyro behavior, i.e., no lock-in.

Therefore, whereas without dither, locking occurs when $a \leqslant b$, with dither locking occurs only when $a \leqslant b\, J_0(c/\omega_d)$. Furthermore, if c/ω_d is a root of J_0 (i.e., $c/\omega_d = 2.405, 5.520, \cdots$), we have $\dot{\psi} = a$, i.e., lock-in vanishes. In practice this is usually not accomplished because the dither may be constrained to oscillate at only certain resonant frequencies and amplitudes.

One way to obtain an alternating bias is the "body dither" which involves oscillating the laser gyro about an axis normal to the plane of the ring. The dithering is usually accomplished by mounting the gyro on a rotational spring system which is oscillated by means of a piezoelectric transducer system. Typical values of c and ω_d are 100 kHz and 400 Hz, respectively. Fig. 4 shows the demodulated beat note versus rotation rate for a sine-wave dithered gyro. Note that there is a finite residual lock band at $\Omega = 0$. This is because the gyro body typically oscillates only at mechanical resonant frequencies and amplitudes with nonzero J_0's in (12). Curiously enough, mechanical noise reduces the width of the lock-in band. Theoretically this can be seen by including a noise term in the dither amplitude of (7) ($c \to c + n$ where n is a pseudo-random noise amplitude that is rapidly varying compared to a dither cycle [10]).

Another successful technique involves the transverse Kerr effect [6], [32]. Here one of the gyro mirrors is coated with a "soft" magnetic material (easily switched). The constant magnetooptic induced bias is alternated at some frequency. As in the body-dither approach, the positive and negative excursions of bias cancel over a cycle and only the rotation rate information appears in the beat note.

It has been shown that a lock-in reduction effect similar to the alternating bias schemes can be obtained by a phase shift modulation technique using optically reciprocal elements in the ring cavity. One such scheme involves two prisms fixed to each other and vibrated as shown in Fig. 5 [33]. The laser gyro output appears frequency modulated as in the alternating bias case.

Finally, we mention a scheme which is based on the fact that backscattered light from the mirrors is a major cause of lock-in. This scheme involves oscillating one of the mirrors in a shear mode parallel to the plane of the ring cavity [34]. The combination of amplitude, direction, frequency, and phasing of the dithering mirror is critical. Lock-in threshold is reduced

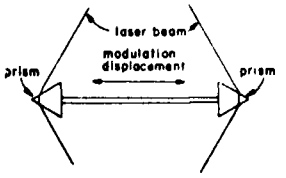

Fig. 5. A dithered effect using reciprocal elements in the ring cavity.

because backscattered light from one mode into the counter-rotating one is Doppler shifted.

In summary, a two-mode ring laser gyro has two counter-rotating running waves. Rotation rate information is obtained from the gyro by observing the beat note between the modes. Ideally, the beat note is linearly proportional to the rotation rate. In practice this is not true because the two modes are coupled by the common nonlinear gain medium and by the scattering of energy from each of the beams into the direction of the other. The result is that at some low rotation rate mode locking occurs giving a zero beat note for a nonzero rotation. Thus, there is dead band (typically 0.1°/s) about zero rotation, which gives no beat note.

Since technological constraints prevent the elimination of the dead band, various procedures have been developed to reduce its effect on gyro operation. Usually these fall into one of two categories, either biased or dithered operation. In biased operation, a constant "artificial" rotation rate is added (e.g., by a Faraday bias) to the input rate so that the locking region is avoided. The rotation rate measurement then depends on the accuracy with which the bias is known. This bias can change owing to varying magnetic fields and temperature. Since the bias value has to be subtracted to obtain the input rotation rate, and since the value of this bias is large compared to the input rotation rate, a small percentage variation in the bias may easily result in an order of magnitude error in the computed rotation rate. In the dithered operation, an alternating bias is used to circumvent the requirement on the absolute stability of the magnitude of the bias. However, any asymmetry in the applied oscillating bias results in null-shift errors. Furthermore, a body-dither gyro does not have the advantages that come with a truly strapped down device.

III. Multioscillator Laser Gyros: ZLAG

A class of multioscillator gyros [35], the differential laser gyro (DILAG) [14], [15] and its generalization, the ZLAG, consists of 2 two-mode ring lasers sharing the same cavity and having orthogonal circular polarizations (see Fig. 6). Bias elements are used, but by taking the difference of the beat notes from the two coresident ring lasers one cancels the bias out and obtains twice the rotation rate sensitivity.

As for the two-mode gyro, an accurate measurement of an input rotation requires the modes to oscillate independently of one another. To help satisfy this requirement, the frequencies of the modes with different polarizations are separated by optical activity. A quartz crystal with its optic axis parallel to the laser axis is often used. In addition, the counterrotating modes are separated by a Faraday bias. The amount of splitting required depends on how successful one is at minimizing

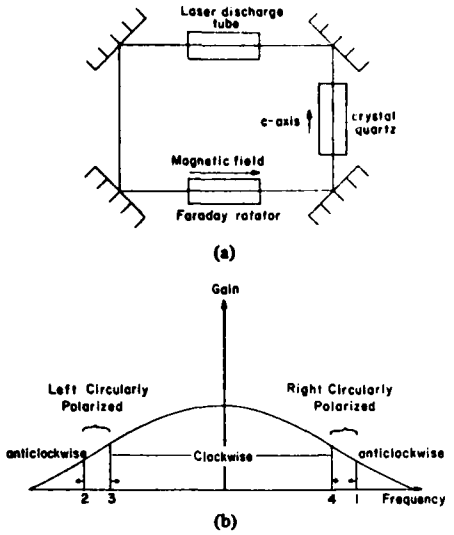

Fig. 6. (a) Physical setup and (b) frequency spectrum of a DILAG.

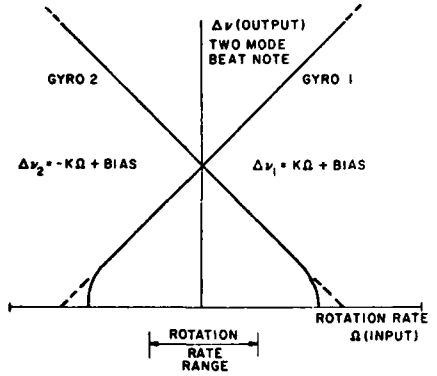

Fig. 7. Beat note versus rotation rate for a DILAG. Note that the bias cancels out in the difference of the beat notes.

backscattering and polarization anisotropies. Typical numbers are 0.5 MHz between counterrotating modes of like polarization and 100 MHz between modes of different polarizations.

Application of an anticlockwise rotation shifts the clockwise modes toward higher frequencies relative to the anticlockwise modes. Fig. 7 shows that the beat note of the left circularly polarized gyro is given by subtracting the anticlockwise from the clockwise frequency; that is,

$$\dot{\psi}_1 - \dot{\psi}_4 = S\Omega + \text{bias} \tag{13}$$

where $\dot{\psi}_i = \nu_i + \dot{\phi}_i$ is the frequency of the ith mode, the rotation rate Ω is positive for anticlockwise rotation, and bias is the frequency bias for the counterrotating mode beat frequencies. This bias is chosen to be positive and much greater than $|S\Omega|$ so as to operate far from lock-in. The beat note for the right circularly polarized gyro is given by subtracting the clockwise-mode frequency from that of the anticlockwise mode

$$\dot{\psi}_3 - \dot{\psi}_2 = S\Omega + \text{bias}. \tag{14}$$

So by subtracting one beat note [see (13)] from the other [see (14)], one cancels the bias and gets twice the sensitivity of one gyro (see Fig. 7).

In the unlocked region, then, the input rotation rate is related to the beat frequencies by

$$\Omega = S^{-1}\left[(\dot{\psi}_3 - \dot{\psi}_2) - (\dot{\psi}_1 - \dot{\psi}_4)\right]. \tag{15}$$

This relation is no longer valid if two or more modes are frequency locked. There are six two-mode locking possibilities and they fall into three distinct categories: 1) locking of unidirectional waves caused by x-y Q or phase anisotropy [19], [20]; 2) locking of bidirectional waves with opposite polarizations caused by backscattering [12] and localized losses [13]; 3) locking of bidirectional waves with the same polarization, which requires backscattering and x-y Q or phase anisotrophy acting simultaneously. In addition to these three locking mechanisms, which arise primarily from mirror imperfections, the nonlinear polarization of the active medium may also cause mode locking [18]. In principle these locking problems can be minimized with sufficient biasing, that is, the introduction of crystal quartz to get rid of the locking of unidirectional modes and the use of the Faraday effect to cure the locking of bidirectional modes. However, because of alignment difficulties and operational instabilities it is advantageous to keep the physical size and complexity of the biasing elements to a minimum.

As in the two-mode laser gyro, nearly equal amounts of Ne^{20} and Ne^{22} are used to reduce mode competition. By operating with an average frequency midway between the two line centers, we avoid the extreme mode competition occurring at line center in the single isotope case. Furthermore, the net frequency pulling nearly vanishes when the isotopic line centers straddle the operating frequencies. Ideally, the laser modes should obtain their gain from different atomic population groups.

We see that the ZLAG can be made to be insensitive to the effects of lock-in and bias instability. There remains the question of how accurately it can determine input rotations. For example, the dispersive behavior of the gain medium may cause null shifts and scale factor changes. The determination of this effect and the search for an optimum ZLAG configuration is the purpose of current experimental and theoretical ZLAG studies. We describe these studies in the following sections.

IV. Semiclassical Theory of a ZLAG

In recent ring laser multioscillator work [16], [18], semiclassical laser theory was found to accurately describe the ZLAG. This theory solves the coupled Maxwell-Schrödinger equations [36], [37]. Self-consistently, each atom in the active medium has an induced electric dipole moment. These dipoles combine to form a macroscopic polarization which drives the laser field. This field in turn induces the dipole moments in the atoms (see Fig. 8). Maxwell's equations describe the driven electromagnetic field and Schrödinger's equation describes the atoms' behavior.

A. Field Equations

For the ZLAG gyro where there are two pairs of counterrotating modes, one with left circular polarization and one with right circular polarization, the electric field is given by

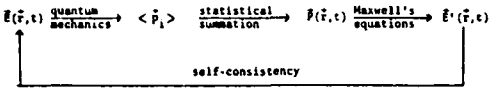

Fig. 8. Electric field E assumed in cavity induces microscopic dipole moments $\langle p_i \rangle$ in the active medium according to the laws of quantum mechanics. These moments are then summed to yield the macroscopic polarization of the medium $\tilde{P}(\tilde{r}, t)$ which acts as a source in the Maxwell's equations. The condition of self-consistency then requires that the assumed field $\tilde{E}$ equals the reaction field $\tilde{E}'$.

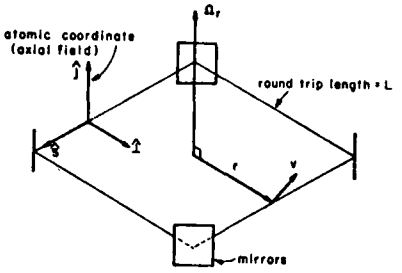

Fig. 9. Ring laser coordinate system.

$$E(s,t) = \tfrac{1}{2}\{E_1(t)\hat{\epsilon}_- \exp[-i(\nu_1 t + \phi_1(t))] + E_2(t)\hat{\epsilon}_+ \exp[-i(\nu_2 t + \phi_2(t))]\} \exp(ik_A s) + \tfrac{1}{2}\{E_3(t)\hat{\epsilon}_- \exp[-i(\nu_3 t + \phi_3(t))] + E_4(t)\hat{\epsilon}_+ \exp[-i(\nu_4 t + \phi_4(t))]\} \exp(-ik_C s) + \text{c.c.} \quad (16)$$

where the subscript $C(A)$ denotes clockwise (anticlockwise) traveling waves, s is the displacement along the laser axis (see Fig. 9), $\nu_n + \dot{\phi}_n$ is the lasing frequency, and E_n and ϕ_n are the slowly varying electric field amplitude and phase. The $\hat{\epsilon}_\pm$ (circularly polarized) unit vectors are defined by $\hat{\epsilon}_\pm = (\hat{x} \pm i\hat{y})/\sqrt{2}$. (For convenience the frequencies are in radians per second when we are dealing with theory and in hertz when we are dealing with the experimental results. We feel that the advantages gained outweigh the risk of confusion.) Table I defines this notation in terms of that used in classical optics. The electric field induces a polarization in the medium

$$P(s,t) = \tfrac{1}{2}\{\mathcal{P}_1(t)\hat{\epsilon}_- \exp[-i(\nu_1 t + \phi_1(t))] + \mathcal{P}_2(t)\hat{\epsilon}_+ \exp[-i(\nu_2 t + \phi_2(t))]\} \exp(ik_A s) + \tfrac{1}{2}\{\mathcal{P}_3(t)\hat{\epsilon}_- \exp[-i(\nu_3 t + \phi_3(t))] + \mathcal{P}_4(t)\hat{\epsilon}_+ \exp[-i(\nu_4 t + \phi_4(t))]\} \exp(-ik_C s) + \text{c.c.} \quad (17)$$

Starting with Maxwell's equations and assuming that the electric field amplitudes and phases are slowly varying in time compared to an optical period, one obtains four equations for the time development of the electric field amplitudes E_n, and four equations for the frequencies $\nu_n + \dot{\phi}_n$. These eight field equations are

$$\dot{E}_n + \frac{1}{2}\frac{\nu_n}{Q_n}E_n = -\frac{1}{2}\frac{\nu_n}{\epsilon_0}\operatorname{Im}(\mathcal{P}_n) \quad (18)$$

and

TABLE I
DEFINITION OF MODE SUBSCRIPTS IN (1) IN TERMS OF RUNNING-WAVE DIRECTION AND CLASSICAL FIELD POLARIZATIONS. ONE RING LASER CONSISTS OF MODES 2 AND 3, I.E., CONSISTS OF LEFT CIRCULAR POLARIZATIONS, AND THE OTHER IS A MADE UP OF MODES 1 AND 4.

Mode subscript	Direction	Unit vector	Classical polarization
1	A (+)	$\hat{\epsilon}_-$	Anticlockwise, right circularly polarized
2	A (+)	$\hat{\epsilon}_+$	Anticlockwise, left circularly polarized
3	C (-)	$\hat{\epsilon}_-$	Clockwise, left circularly polarized
4	C (-)	$\hat{\epsilon}_+$	Clockwise, right circularly polarized

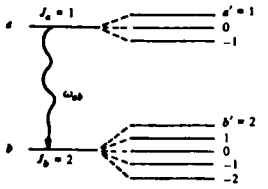

Fig. 10. Possible level scheme. The electronic quantum numbers for the upper and lower levels are a and b, respectively; the magnetic numbers are a' and b'; ω_{ab} is the frequency difference between the levels in the absence of a magnetic field; $\omega_{a'b'}$ is the frequency difference between magnetic sublevels a' and b'. This level diagram with $J_a = 1$, $J_b = 2$ corresponds to the 1.15, 3.39, and 0.6329 μm Ne lines in the He–Ne laser.

$$\nu_n + \dot{\phi}_n = \Omega_n - \frac{1}{2}\frac{\nu_n}{\epsilon_0 E_n}\operatorname{Re}(\mathcal{P}_n) \quad (19)$$

where $n = 1, 2, 3$, and 4. In (18) the second term on the left-hand side (LHS) represents the losses present in the passive cavity and the polarization appears on the RHS in the form of a driving term. From (19) we see that the lasing frequency $\nu_n + \dot{\phi}_n$ is the sum of Ω_n, the passive cavity frequency, and a term arising from the dispersive behavior of the active medium .

B. Polarization of the Active Medium

To determine the $\mathcal{P}_n$'s in (17) we treat the atoms quantum mechanically, including the following features:

1) the medium has an arbitrary amount of inhomogeneous broadening
2) the atomic levels have nonzero angular momenta (see Fig. 10)
3) the electromagnetic field has two polarization components
4) a magnetic field may be applied
5) two isotopes contribute to the gain.

Atoms with different velocities can readily be described by a population matrix which is a density matrix whose trace is the number of atoms/volume [37]. We assume that the atoms have a Maxwell-Boltzmann velocity distribution. Points 2)-4) require a vector theory which leads to an additional selection rule, $\Delta m = \pm 1$, governing transitions between the magnetic sublevels. Contributions from different isotopes are different because of differences in the position of the atomic line centers, average speed, and Doppler width. We account for 5) by taking the average of the macroscopic variables from the different isotopes.

We solve for the population operator by iterating the Schrödinger equation to third order in the interaction energy $-er \cdot E$.

The resulting expression is coupled to the field equations via the electric field amplitude and phase. Since the effect of any one atom on the field in the cavity is minute, the field varies little over the lifetime of an atom. This allows us to treat the electric field amplitudes E_n and phases ϕ_n (where the optical frequency oscillations are already factored out) as constants in the atomic equation. This is an important step which decouples the atomic equation from the field equations and makes the integration of the atomic equation possible.

The polarization obtained in this fashion contains terms linear and cubic in the electric field amplitudes. The real and imaginary parts of the linear terms give the mode pulling and linear gain, respectively. They are [18]

$$\alpha_n = \nu\bar{N}/(\hbar Ku\epsilon_0) \sum_i f_i \sum_{a'} \sum_{b'} \delta_{a',b'+p_n} |\mathcal{P}_{a'b'}|^2 \cdot Z_i[\gamma_{ab} + i(\omega_{a'b'} - \nu_n)] - \nu/(2Q_n) \tag{20}$$

$$\sigma_n = \nu\bar{N}/(\hbar Ku\epsilon_0) \sum_i f_i \sum_{a'} \sum_{b'} \delta_{a',b'+p_n} |\mathcal{P}_{a'b'}|^2 \cdot Z_r[\gamma_{ab} + i(\omega_{a'b'} - \nu_n)] \tag{21}$$

where

$\nu = \frac{1}{4} \sum_{n=1}^{4} \nu_n$
$\hbar$ = Planck's constant/(2π)
ϵ_0 = the permittivity of vacuum
Ku = the Doppler width
$p_n = 1$ for $n = 2$ and 4
$p_n = -1$ for $n = 1$ and 3
γ_{ab} = the electric dipole decay rate
Z_r, Z_i = the real and imaginary parts of the plasma dispersion function
$\mathcal{P}_{a'b'} = \langle a'|er|b'\rangle$, the electric dipole matrix element between levels a' and b'
$\bar{N} = (1/L) \int_0^L N(s, t)\, ds$
$N(s, t)$ = the excitation at position s
f_i = the fractional abundance of the ith isotope.

The third-order coefficients are more complicated. They are tractable in the strong Doppler limit [18] (where the Doppler width is much larger than the homogeneous linewidth and the detuning). As discussed, for example, in [37], the third-order contribution to $\dot{E}_n$ has the form

$$\dot{E}_n^{(3)} = -\sum_\mu \sum_\rho \sum_\sigma E_\mu E_\rho E_\sigma \operatorname{Im}\{\vartheta_{n\mu\rho\sigma} \exp(i\psi_{n\mu\rho\sigma})\}$$

where the relative phase angle $\psi_{n\mu\rho\sigma} = (\nu_n - \nu_\mu + \nu_\rho - \nu_\sigma)t + \phi_n - \phi_\mu + \phi_\rho - \phi_\sigma$. The complex third-order saturation coefficients $\vartheta_{n\mu\rho\sigma}$ contain three time integrals, a velocity integral, a spatial integral, four sums over magnetic sublevels, and a sum over isotopic abundances f_i:

$$\vartheta_{n\mu\rho\sigma} = \sum_i f_i \sum_{a'} \sum_{b''} \sum_{a''} \sum_{b'} \frac{1}{L} \int_0^L ds \int_{-\infty}^{\infty} dv \int_0^{\infty} d\tau' \cdot \int_0^{\infty} d\tau'' \int_0^{\infty} d\tau''' \{\cdots\}.$$

TABLE II

SUMMARY OF THE $\vartheta_{n\mu\rho\sigma}$ CALCULATION WHICH YIELDS THE COEFFICIENTS GIVEN IN (9)–(17). THE DIRECTION AND CHANGE IN THE MAGNETIC QUANTUM NUMBER ARE INDICATED BY d_n AND p_n. THE MAGNETIC SUBLEVEL TRANSITIONS ARE GIVEN BY THE DASHES IN COLUMN 8. A LEFT (RIGHT) SLANTING DASH (\) (/) INDICATES A CHANGE IN THE MAGNETIC QUANTUM NUMBER OF −1 (+1). THE NINTH COLUMN INDICATES THE θ_{nm} TO WHICH THE PARTICULAR $\vartheta_{n\mu\rho\sigma}$ BELONGS.

nμρσ	d_μ	d_ρ	d_σ	Integral Type	d_n	p_n	Transitions	θ_{nm}
1111	+	+	+	1	+	−	\\\	11
2222	+	+	+	1	+	+	///	22
3333	−	−	−	1	−	−	\\\	33
4444	−	−	−	1	−	+	///	44
1122	+	+	+	1	+	−	/\\	12
1221	+	+	+	1	+	−	\//	12
2211	+	+	+	1	+	+	/\\	21
2112	+	+	+	1	+	+	\\/	21
3344	−	−	−	1	−	−	/\\	34
3443	−	−	−	1	−	−	\//	34
4433	−	−	−	1	−	+	/\\	43
4334	−	−	−	1	−	+	\\/	43
1133	+	−	−	3	+	−	\\\	13
1331	−	−	+	2	+	−	\\\	13
3311	−	+	+	3	−	−	\\\	31
3113	+	+	−	2	−	−	\\\	31
2244	+	−	−	3	+	+	///	24
2442	−	−	+	2	+	+	///	24
4422	−	+	+	3	−	+	///	42
4224	+	+	−	2	−	+	///	42
2233	+	−	−	3	+	+	/\\	23
2332	−	−	+	2	+	+	\\/	23
3322	−	+	+	3	−	−	/\\	32
3223	+	+	−	2	−	−	\//	32
1144	+	−	−	3	−	−	/\\	14
1441	−	−	+	2	−	−	\//	14
4411	−	+	+	3	+	+	/\\	41
4114	−	−	+	2	+	+	\\/	41

TABLE III

SUMMARY OF THE COEFFICIENTS OF THE TERMS CONTAINING PHASE ANGLES. INTEGRAL TYPES 2 AND 3 VANISH IN THE DOPPLER LIMIT.

nμρσ	d_μ	d_ρ	d_σ	Integral Type	d_n^{+-}	p_n^{+-}	Transitions	Phase Angle
1243	+	−	−	3	+	−	\//	+ψ
1342	−	−	+	2	+	−	/\\	
2134	+	−	−	3	+	+	\\/	−ψ
2431	−	−	+	2	+	+	/\\	
3421	−	+	+	3	−	−	\//	−ψ
3124	+	+	−	2	−	−	/\\	
4312	−	+	+	3	−	+	\\/	+ψ
4213	+	+	−	2	−	+	/\\	

In general, various selection rules yield only one mode n for a given combination of the indexes μ, ρ, and σ. In the present four-mode problem, out of $4^3 = 64$ possible combinations, the conservation of angular momentum ($\Delta m = \pm 1$) for axial magnetic fields and the conservation of the wave vector ($\Delta k = 0$) reduce the number to 36 terms with $\psi_{n\mu\rho\sigma} = 0$ (see Table II) and 8 with $\psi_{n\mu\rho\sigma} = \pm\psi$ (see Table III). The information in these tables has been programmed into a computer in even greater generality than that needed here. For example, the programs can also treat hyperfine structure, which does not occur in Ne^{20}-Ne^{22} mixtures. The general $\vartheta_{n\mu\rho\sigma}$ are defined in [16]. While they are exceedingly complicated from an analytical point of view, they are relatively easy to deal with using a computer.

For a number of simple illustrations, see [18]. There the programs are used to calculate intensity-tuning curves and other features of Zeeman ring lasers operating without cavity anisotropy, with single-isotope media and in the Doppler limit. In the ZLAG problem, these simplifications cannot be used. In addition, we now consider possible off-axis magnetic fields, for which a given circular polarization can cause $\Delta m = \pm 1, 0$, rather than just one of the three values. Inclusion of these features gives us a fairly realistic model of the atom-field interaction in a ZLAG near threshold. The use of third-order perturbation theory causes saturation effects to be overestimated for higher intensity operation.

C. Backscattering and Cavity Anisotropies

In this section we show how the mode-locking mechanisms of backscattering, localized losses x-y Q, and phase anisotropies are incorporated into the amplitude and frequency determining equations. We begin by treating the case of x-y Q and phase anisotropies, that is, where the losses and phase shift per cavity roundtrip for an x polarized wave (see Fig. 9) are different from those for a y polarized wave. The main contribution to these anisotropies is reflection from mirror surfaces at angles other than normal incidence. An originally right circularly polarized wave has a left circularly polarized component added to it after a reflection and vice versa. This leads to the introduction to the amplitude- and frequency-determining equations with the terms

$$(\dot{E}_n)_{xy} = \left[\frac{c}{L}\frac{\phi_y - \phi_x}{2}\sin\psi_{nm} - \frac{c}{L}\frac{l_y - l_x}{2}\cos\psi_{nm}\right]E_m$$

and

$$(\dot{\psi}_n)_{xy} = \left[\frac{c}{L}\frac{\phi_y - \phi_x}{2}\cos\psi_{nm} + \frac{c}{L}\frac{l_y - l_x}{2}\sin\psi_{nm}\right]\frac{E_m}{E_n} \tag{22}$$

where

$n, m = 1,2; 2,1; 3,4; 4,3$
$\psi_{nm} = \psi_n - \psi_m$
ϕ_x and ϕ_y = the phase shifts added onto the s and p waves per roundtrip
l_xE_x and l_yE_y = the losses of the s and p waves per roundtrip
c = the velocity of light
L = the cavity length.

With a 1 percent output coupling and a cavity length of 30 cm, $(c/L)l_x = 10$ MHz. So if $l_x/l_y \simeq 0.9$, the Q anisotropy coefficient $(c/L)(l_y - l_x)/2 \simeq 1$ MHz. The phase anisotropy is not as predictable because mirrors from different coating runs exhibit different birefringent behavior for nonnormal incidence. At the present state of the art, a multilayer dielectric mirror coated for maximum reflection at a 45 percent angle of incidence may have $|\phi_y - \phi_x| \simeq 5 \times 10^{-2}$ rad/reflection. This leads to a phase anisotropy coefficient of 200 MHz. The lock-in threshold (proportional to the minimum measurable rotation rate) equals the product of the anisotropy coefficient and the sum or difference of electric-field amplitude ratios. For example, looking at the frequency difference between the unidirectional modes 1 and 2 we have

$$(\dot{\psi}_{12})_{xy} = \frac{c}{L}\frac{\phi_y - \phi_x}{2}\left[\frac{E_2}{E_1} - \frac{E_1}{E_2}\right]\cos\psi_{12} + \frac{c}{L}\frac{l_y - l_x}{2}\left[\frac{E_2}{E_1} + \frac{E_1}{E_2}\right]\sin\psi_{12}. \tag{23}$$

Referring to the earlier discussion involving (6), we see that the lock-in threshold is proportional to the coefficients of the cosine and sine terms. Of particular interest is the $(E_1/E_1 - E_1/E_2)$ factor in the phase anisotropy contribution to (23). This is because the phase anisotropy coefficient produces the largest mode coupling by far, and can yield a lock-in threshold as high as 200 MHz. However, one can cancel its effect by operating the gyro with close to equal unidirectional field amplitudes.

Locking of modes with different polarizations and opposite directions is caused by backscattering. Right (left) circularly polarized light is scattered into the opposite direction because of imperfections of optical surfaces and to a lesser extent by dust particles in the cavity. The scattered light becomes left (right) circularly polarized, and it alters the frequency and amplitude of the left (right) circularly polarized counterrotating mode. This leads to the following terms in the amplitude- and frequency-determining equations:

$$(\dot{E}_n)_s = -b_m E_m \cos(\psi_n - \psi_m - \epsilon_m)$$
$$(\dot{\psi}_n)_s = b_m \frac{E_m}{E_n}\sin(\psi_n - \psi_m - \epsilon_m) \tag{24}$$

where

$n, m = 1,3; 3,1; 3,1; 2,4; 4,2$
$b_m E_m$ = the rate of increment in the amplitude of the backscattered wave
ϵ_m = the phase shift given to the backscattered part of the wave.

The percentage of light backscattered from one mode into the solid angle of the oppositely directed mode is estimated to be 1×10^{-6}. This gives a backscattering coefficient $b_m = 100$ Hz.

Localized losses also cause locking of modes with different polarizations and directions. This is because a standing wave with nodes at the positions where the losses occur (usually at the mirrors) may experience less net loss than a running wave and, therefore, may have a greater chance of being above threshold. Since the terms describing lock-in via localized losses have the same form as those describing backscattering [13], we may, to a good approximation, account for it by changing b_m in (24). Experiments with two-mode gyros set this value at around 500 Hz.

Locking of modes having the same polarization and opposite direction requires both backscattering and $x - y$ Q or phase anisotropy acting simultaneously. The corresponding coefficient for this case is

$$b_m\frac{(l_y - l_x)}{2} \quad \text{or} \quad b_m\frac{(\phi_y - \phi_x)}{2}.$$

This rate is three orders of magnitude less than the back-

scattering and localized losses coefficient, and six orders of magnitude less than the x - y Q or phase coefficient. Therefore, we expect that the coupling of the modes 1, 4 and 2, 3 is negligible.

D. Frequency and Amplitude Determining Equations

In Section IV-B we showed how one can determine the macroscopic polarization of the active medium by using quantum mechanics, and in Section IV-C we showed how the various mode coupling mechanisms may be incorporated into the theory. Use of these results in the field (18) and (19) leads to the following amplitude equations:

$$\dot{E}_n = E_n\left(\alpha_n - \sum_{m=1}^{4}\theta_{nm} I_m\right) - \mathrm{Im}\{(\vartheta_{nijk} + \vartheta_{nkji})\exp(i\psi_{nijk})\}E_iE_jE_k + \frac{c}{2L}E_i[(\phi_y - \phi_x)\sin\psi_{ni} - (l_y - l_x)\cos\psi_{ni}] - b_kE_k\cos(\psi_{nk} - \epsilon_k) \quad (25)$$

and

$$\nu_n + \dot{\phi}_n = \Omega_n + \sigma_n - \sum_{m=1}^{4}\tau_{nm} I_m - \mathrm{Re}\{(\vartheta_{nijk} + \vartheta_{nkji})\exp(i\psi_{nijk})\}E_iE_jE_k/E_n + \frac{c}{2L}\frac{E_i}{E_n}[(\phi_y - \phi_x)\cos\psi_{ni} + (l_y - l_x)\sin\psi_{ni}] + b_k\frac{E_k}{E_n}\sin(\psi_{nk} - \epsilon_k) \quad (26)$$

where n, i, j, k are 1, 2, 4, 3; 2, 1, 3, 4; 3, 4, 2, 1; 4, 3, 1, 2. Here σ_n is the linear mode pulling; the self-saturation coefficients $\beta_n \equiv \theta_{nn}$ and the self-pushing coefficients $\rho_n \equiv \tau_{nn}$ are defined by $\rho_n + i\beta_n = \vartheta_{nnnn}\, 2\hbar^2\gamma/\mathcal{P}^2(\gamma_a^{-1} + \gamma_b^{-1})$, the cross-saturation θ_{nm} and cross-pushing coefficients τ_{nm} $(n \neq m)$ are defined by $\tau_{nm} + i\theta_{nm} = (\vartheta_{nnmm} + \vartheta_{nmmn})\, 2\hbar^2\gamma/\mathcal{P}^2(\gamma_a^{-1} + \gamma_b^{-1})$, the dimensionless intensities $I_m = (\mathcal{P}E_m/\hbar)^2(\gamma_a^{-1} + \gamma_b^{-1})/2\gamma$ and $\mathcal{P}$ is the reduced matrix element for the transition (see [37]). These equations contain terms with four-mode relative phase angles ψ_{nijk} of the electric field. These terms arise from the nonlinear behavior of the gain medium in the presence of four optical modes. Finally, we have the contributions from the x-y phase and Q anisotropy and from backscattering and localized losses. The eight amplitude and frequency determining equations are written explicitly in Appendix I.

V. Special Cases

A. Steady-State Operation Outside the Lock-In Region

Equations (25) and (26) are coupled by terms containing the relative phases. If we are only interested in the accuracy of ZLAG measurements outside the lock-in regions, then all four modes oscillate independently of one another, and the terms containing the relative phases average to zero. As a result, the set of amplitude equations are to a good approximation uncoupled from the set of frequency equations. It should be noted that if accuracies of the order of 10^{-3} Hz, which is now achievable in laser gyros, are involved, this decoupled approximation may not be valid. In addition, we are usually interested only in the cases where all four electric-field amplitudes are above threshold and at steady state. Consequently, the problem reduces to solving the four algebraic equations

$$\left(\alpha_n - \sum_{m=1}^{4}\theta_{nm} I_m\right) = 0 \quad (27)$$

simultaneously for the intensities I_m. These values are then used in the frequency equations

$$\nu_n + \dot{\phi}_n = \Omega_n + \sigma_n - \sum_{m=1}^{4}\tau_{nm} I_m \quad (28)$$

to determine the lasing frequencies.

This model for the ZLAG is programmed for running on a Data General Eclipse Computer. The steady-state intensities are obtained by solving the intensity equations using a Gauss-Jordan matrix-inversion method. The 16 possible solutions are tested for stability using a small-vibrations analysis [37]. The programs include interactive input/output and plotting routines which greatly facilitate the study of our many parameter model.

To summarize, the features of our ZLAG model are: the cavity has four circularly polarized running-wave modes; the medium is inhomogeneously broadened with atomic levels of arbitrary angular momentum and hyperfine structure; it is possible to have more than one isotope and to have an applied magnetic field.

B. Reduction to Four Weakly Coupled Single-Mode Oscillators

In general, the ZLAG is a coupled four-mode problem. This section examines the extent in which the ZLAG may be treated as four weakly coupled single-mode oscillators. Examination of (25) and (26) shows that this requires: 1) the effects of cavity anisotropies be small, 2) the phase angle (ψ_{nijk}) terms be negligible, and 3) the cross-saturation coefficients be small relative to the self-saturation coefficients.

Requirements 1) and 2) are satisfied when the mode frequencies are not locked to one another. As discussed in Section V-A, this is so under normal operating conditions. Requirement 3) concerns the size of the two-mode coupling constants

$$C_{nm} = \theta_{nm}\theta_{mn}/\beta_n\beta_m. \quad (29)$$

These constants are the ratios of the cross-saturation coefficients to the self-saturation coefficients and represent a normalized measure of two-mode coupling [37]. In the limit of $C_{nm} = 0$, there is no coupling between the nth and mth modes. The ZLAG can be made to have the C_{nm}'s substantially less than 1 and hence to approximate the ideal uncoupled limit. To find this configuration, we consider the results in [18]. There are six coupling constants: $C_{12}, C_{13}, C_{14}, C_{23}, C_{24}, C_{34}$. For the two-isotope gyro tuned midway between the isotopic line centers, the largest of these are by far the unidirectional constants C_{12} and C_{34}. The Bennett holes for a given unidirectional pair can overlap considerably. However, the coupling is

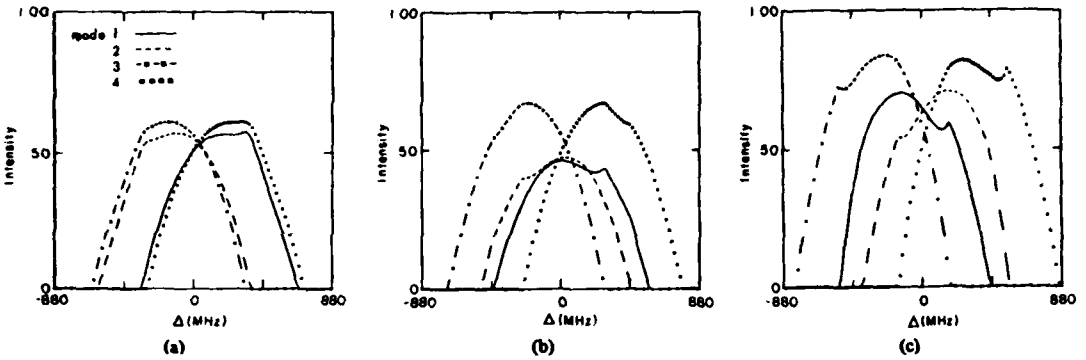

Fig. 11. Intensities of the four ZLAG mode versus detuning for an axial magnetic field of (a) 10 G, (b) 50 G, and (c) 100 G. Detuning is the difference between the mean of the four ZLAG frequencies and the midpoint of the two Ne isotopic line centers. An axial magnetic field is sometimes applied on the laser plasma to bias the counterrotating modes. We assumed the strong Doppler limit when generating these curves. The optical activity bias is 166 MHz, γ_a = 13 MHz, γ_b = 27 MHz, γ = 172 MHz, N/N_T = 1.2.

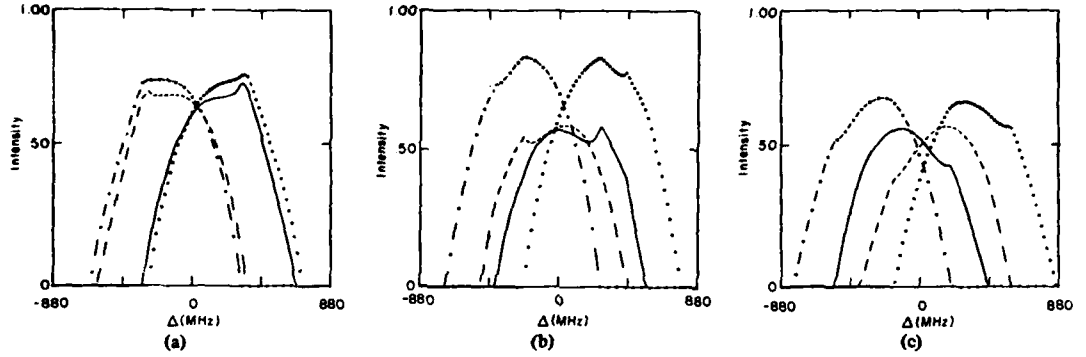

Fig. 12. Intensities of the four ZLAG modes versus detuning for an axial magnetic field of (a) 10 G, (b) 50 G, and (c) 100 G. We did not invoke the strong Doppler limit when generating these curves. All other parameters are the same as those in Fig. 11.

also influenced by the different matrix element combinations that enter into the cross-saturation and self-saturation coefficients. Specifically, for the $J = 1 \rightarrow 2$ transitions (Ne 632.8 nm, 1.153 μm, and 3.39 μm), the maximum value for the coupling parameter is 0.228 [18]. As seen from [37, Fig. 12-4b], this coupling is small enough to give only minor modifications to the single-mode intensity-versus-tuning curves. On the other hand, $J = 1 \rightarrow 0$ transitions (e.g., Ne 1.53 μm) have a corresponding coupling constant of unity [18] leading to substantial mode interaction and suppression [31, Fig. 12-4a]. As expected, the $J = \frac{1}{2} \rightarrow \frac{1}{2}$ transition has no coupling at all (that is, $C = 0$) because of conservation of angular momentum.

The four bidirectional coupling constants (C_{13}, C_{14}, C_{23}, and C_{24}) contain squares of Lorentzians having detunings of about 400 MHz for the midtuned, two-isotope Ne 632.8 nm line [18]. With an electric-dipole decay constant $\gamma \simeq 2\pi x$ 100 MHz, this gives 1/289 for C and, hence negligible coupling. In addition, C_{23} and C_{14} contain factors of different matrix-element combinations that reduce C by an order of magnitude for the $J = 1 \rightarrow 2$ transitions [18].

Therefore, the ZLAG, when operating outside the lock-in region on the Ne 632.8 nm line ($J = 1 \rightarrow 2$), behaves as though its four modes oscillate nearly independently of one another.

C. *The Strong Doppler Limit*

The strong Doppler limit is valid when the Doppler width Ku is much greater than the decay rates and detuning (K is the laser field wave vector and u is the average atomic velocity). In this limit, the calculation of the third-order coefficients is greatly simplified and the computer time required for running our ZLAG program is cut in half. Unfortunately, since the ZLAG operates midway between the two Ne isotopic line centers, the detuning roughly equals the Doppler width. Using the strong Doppler limit in this case over estimates the mode competition effects. However, for certain cases the strong Doppler limit still gives a good description of ZLAG behavior. For instance, Figs. 11 and 12 show that the tuning curves given by the strong Doppler limit and "exact" theories are essentially equal for a wide range of magnetic fields. On the other hand, Figs. 13 and 14 show that the strong-Doppler-limit beat note deviates increasingly from the "exact" beat-notes as the magnetic field is increased. Thus, although the strong Doppler limit gives good estimates of the intensities, it is not reliable in predicting the beat note. In fact, for certain configurations, the predicted beat notes may differ in sign as well as in magnitude.

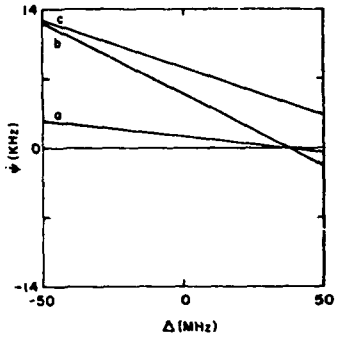

Fig. 13. ZLAG beat note versus detuning, Δ, for an axial magnetic field of (a) 10 G, (b) 50 G, (c) 100 G. Input rotation rate is zero, optical activity bias is 166 MHz, and we used the strong Doppler limit. All other parameters are the same as those in Fig. 11.

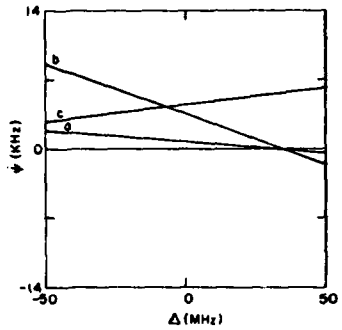

Fig. 14. Beat note versus detuning for an axial magnetic field of (a) 10 G, (b) 50 G, and (c) 100 G. All other parameters are the same of those in Fig. 13 except we did not invoke the strong Doppler limit.

VI. ZLAG Experiments

A. Experimental Apparatus

This section describes the ZLAG experimental apparatus and results performed to test the theory. Specifically, Section VI-A describes the apparatus; Section VI-B describes the effects of axial magnetic fields on counterrotating modes; Section VI-C describes the ZLAG beat note; and Section VI-D describes the current state of the ZLAG. The cavities used were constructed from solid blocks of CerVit. Machined into each of these blocks are clearance holes, gain bores, and apertures to accommodate both the optical and electrical discharge paths. Both mirrors and electrodes are affixed to polished surfaces on the blocks. The CerVit blocks in each case have two separate, equal gain regions. The electrodes (one cathode and two anodes) are positioned so as to cancel the Langmuir flow effects from the dc excited plasma gain media flow. Each block has a valved tip-off connection allowing easy attachment or removal from a vacuum fill station. The gas fill parameters are quickly changeable at will. Each of these instruments has a port access to the laser beam optical path where a quartz crystal biasing element may be positioned. Some of the instruments have magnetic coils around the plasma gain section providing a variable magnetic field along the optic axis.

Fig. 15. Out-of-plane ring laser gyro.

Alignments of both mirrors and crystal are done with the instrument lasing while attached to a vacuum fill station. The seals on both the mirrors and crystal assembly are wax which softens when heated. The lifetime expectancy of most of these wax sealed instruments is only a few days without an activated getter. The mirrors are positioned for maximum intensity output which ensures minimum loss from misalignment. The crystal orientation is adjusted for maximum circularity of polarization of the output modes. This ensures that the optic axis of the crystal and optic axis of the ring laser are parallel.

The crystals used are right handed, i.e., the right circularly polarized modes are higher in frequency than the left circularly polarized modes, with antireflection coatings on polished faces nominally perpendicular to the crystals' rotary axes. The laser gain medium and wavelength is He-Ne and 6328 Å. The cavity length is approximately 30 cm.

As discussed in Sections II-D and III, anisotropic reciprocal optical biasing is needed to avoid x-y mode locking. As is now recognized [38], [39], this type of frequency splitting may be obtained without the use of a material element in the cavity. For example, an out-of-plane ring cavity is implicitly anisotropic. A photograph of such a ring laser cavity is shown in Fig. 15. The four mirror angles of incidence on this instrument are all equal and approximately 15°. A Jones matrix analysis of this cavity as well as our experimental results show an approximate 70 MHz frequency splitting between the left and right circularly polarized modes.

B. Effect of Axial Magnetic Field on Counterrotating Modes

To avoid locking of the counterrotating waves, Faraday rotators are often used to split the counterrotating mode frequencies. Another source for this biasing is given by the Zeeman effect on the active medium itself. Again, as discussed in Section III, the magnitude of the bias must be much larger than the largest expected value of $S\Omega$. This, in effect, limits the rotation rate range. Fig. 16 is a graph of the Faraday induced beat note between modes of like polarization as a function of magnetic field on the active gain plasma of one of these instruments. This instrument has 8 cm of active plasma. Using this graph one calculates a Verdet constant associated with the HeNe gas plasma of approximately 300 Hz/cm · G.

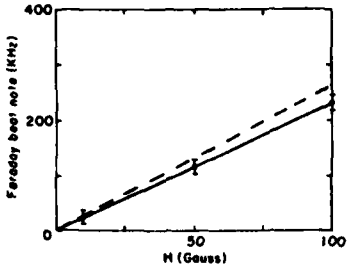

Fig. 16. Faraday beat note from an axial magnetic field on the He-Ne plasma. The dash curve is the theoretically predicted bias. Optical activity is 440 MHz.

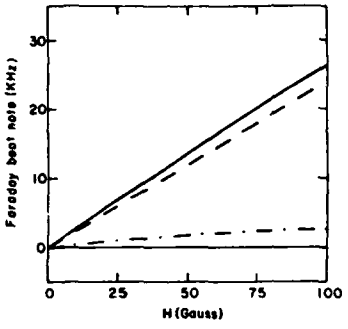

Fig. 17. The Faraday bias (solid curve) may be broken into the mode pulling (dash curve), self mode pushing (dot curve), and cross mode pushing (dot dash) contributions.

This graph does not vary significantly as a function of total gas pressure between 2.5 and 3.5 torr. Likewise, it is not affected by plasma current over an operating range of 2-5 mA. These data were obtained using equal portions of the two isotopes Ne^{20} and Ne^{22} with the mean lasing frequency of the four laser modes being approximately midway between the natural frequencies of the two isotopes.

Also shown, Fig. 16 is the theoretically predicted Faraday bias. According to Fig. 17, frequency pulling accounts for most of the bias. To estimate this pulling contribution we note that a magnetic field H changes the atomic line center according to

$$\omega_{a'b'} = \omega_0 + \mu_B (H/\hbar) g (a' - b') \tag{30}$$

where ω_0 is the zero field frequency, μ_B is the Bohr magneton, g is the Landé g factor, and a' and b' are magnetic sublevel indexes. This alters the frequency-pulling coefficient through changes in the plasma dispersion function [see (21)], as is approximated by

$$\sigma_n \propto Z_r [\gamma_{ab} + i(\omega_0 - \nu_n)] + p_n (\mu_B/\hbar) Hg \cdot \frac{\partial Z_r(\xi)}{\partial \xi}\bigg|_{\xi=\gamma_{ab}+i(\omega_0-\nu_n)} \tag{31}$$

where $p_n = +1$ for $n = 2, 4$ and $p_n = -1$ for $n = 1, 3$. Using (31) to calculate the mode pulling difference $\sigma_4 - \sigma_1$ between counterrotating modes, we find an approximate value due to frequency pulling:

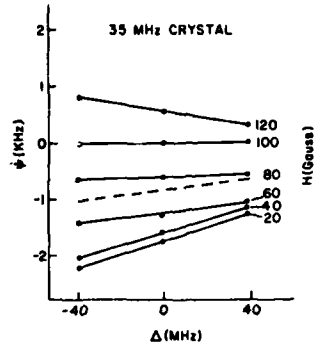

Fig. 18. Four-mode beat note versus detuning for different values of axial magnetic fields. The values of axial magnetic field is shown on the right vertical axis. This gyro has a 35 MHz quartz crystal in the cavity. These data are taken at earth rotation rate. Note that at 80 gauss the slope of the curve is approximately zero. The dash curve is the theoretical result for $H = 80$ G.

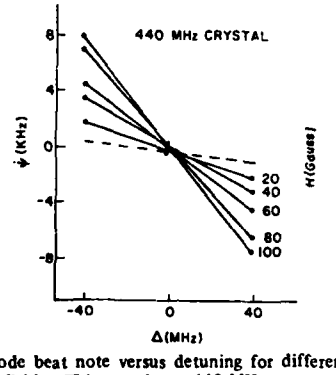

Fig. 19. Four-mode beat note versus detuning for different values of axial magnetic fields. This gyro has a 440 MHz quartz crystal in the cavity. This data is taken at the earth rotation rate. The dash curve is the theoretical result for $H = 20$ gauss.

$$\sigma_4 - \sigma_1 \propto \mu_B \frac{Hg}{\hbar} \frac{\partial Z_r(\xi)}{\partial \xi}\bigg|_{\xi=\gamma_{ab}+i(\omega_0-\nu)} \tag{32}$$

where

$$\nu = \frac{1}{4}\sum_{n=1}^{4} \nu_n$$

and

$$\omega_0 - \nu_4 \simeq \omega_0 - \nu_1.$$

One sees in Fig. 16 that the more exact theoretical curve overestimates the Faraday bias by about 10 percent.

C. ZLAG Beat Note

The following parameter variation data represent an example of many experiments designed to determine the effects of various phenomena on multioscillator gyro performance. Figs. 18 and 19 illustrate the choice of two separate magnitudes of frequency splitting between the left and right circularly polarized modes in a ZLAG. The data were obtained using the gyro described in Section VI-A. The left-right frequency splitting in this instrument was obtained using a quartz crystal

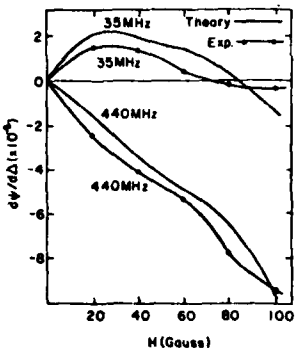

Fig. 20. Slope of multioscillator beat note with respect to detuning versus magnetic field for quartz crystals of 35 and 440 MHz. The experimental values are obtained from Figs. 19 and 20. The theoretical values are the result of a numerical analysis based on the Zeeman laser gyro theory.

placed inside the laser cavity. The vertical axis in the figures represents the multioscillator beat note $\dot{\psi}$ (10 Hz $\simeq$ earth rate for this instrument). All of this data was obtained at the earth rotation rate. Therefore, any substantial beat note other than 10 Hz represents an error in the gyro output. The horizontal axis represents tuning of the mean optical frequency of all four lasing modes. Zero detuning is taken to be midway between the natural 6328 Å transition frequencies of the two gas isotopes (Ne^{20}/Ne^{22}) comprising the gain medium. The detuning is varied by changing the cavity length. The magnitude of the magnetic field strength on the gas plasma is indicated to the right of each curve in each figure. This field is created by magnetic coils wrapped around the gain sections of the laser (see Fig. 15). Fig. 18, associated with 35 MHz frequency splitting by the crystal, indicates a large sensitivity to magnetic field strength at zero detuning. Note that at 80 gauss there is practically no detuning sensitivity in the beat note. Fig. 19, which is for Δ_A = 440 MHz, shows a large cavity length detuning sensitivity for all of the magnetic field strengths. Clearly, the choice of 35 MHz frequency splitting between the left and right circularly polarized models and an axial field of 80 gauss is better than any of the other ZLAG configurations shown in Figs. 18 and 19. It is significant that the results from the theoretical model and these data agree over a wide range of magnetic field (see Fig. 20).

D. Current Status

In summary, the ZLAG minimizes the effects of lock-in without employing moving mechanical components and intercavity optical elements. This is accomplished by using an out-of-plane cavity and by subjecting the plasma to an axial magnetic field. However, this field induces frequency pulling and pushing effects which cause the gyro beat note to be sensitive to cavity length and magnetic field fluctuations. This was predicted by our theory and was shown experimentally to be true for gyros having 440 and 30 MHz polarization biases.

Current research is geared towards finding a ZLAG configuration for which the beat note is sufficiently insensitive to cavity length and magnetic field fluctuations. Our theoretical model indicates that certain optimal combinations of polarization bias and magnetic field may exist. Guided by this model, the developmental studies toward an operational ZLAG laser gyro continue.

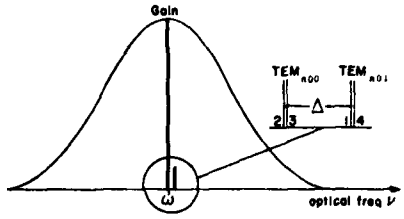

Fig. 21. Spectrum of proposed scalar laser gyro. Modes 2 and 3 are oscillating far above threshold, while modes 1 and 4 are oscillating slightly above threshold. The two sets of modes belong to different transverse modes and are separated in frequency by $\Delta \simeq 60$ MHz [42].

VII. Novel Multioscillator Approaches to Lock-In Threshold Reduction

As discussed in Section II, gyros often use body-shake dither to eliminate the lock-in problem. This method has the same problems of mechanical supports as the conventional gyro. The ZLAG is a clever, purely optical way of circumventing the lock-in region but has an additional problem of lock-in due to polarization anisotropies. In a number of papers [40]-[44], other multioscillator approaches to solving the locking problem were investigated. These schemes pump a traditional linearly polarized ring laser hard enough so that two strong modes and two weak modes oscillate in the cavity (see Fig. 21). The nonlinear interaction between the gain medium and the four laser modes provides mechanisms which reduce the lock-in threshold. The two strong modes are numbered 2 and 3; the two weak modes are numbered 1 and 4. Modes 1 and 2 are anticlockwise modes, while 3 and 4 are clockwise modes. Modes 1, 4 and 2, 3 may have different longitudinal modes or different transverse indexes. For example, the cavity may contain two TEM_{00q} and two TEM_{01q} modes.

A semiclassical laser theory [36], [45] of this scalar multimode ring laser yields amplitude and frequency determining equations like (25) and (26), but without the x-y anisotropy terms and with different values of the coefficients and ordering of the indexes ($nijk$ = 1234, 2134, 3412, 4321). In this section we discuss two useful approaches to solving these equations, called "optical dither" [41] and "2+2" [42]-[44]. These cases resulted from interpretating four-mode data revealing reductions and even elimination of the locking region. For optical dither, consider a configuration that fixes the weak modes to a frequency difference of ω_d. Then the beat note between the strong modes is

$$\dot{\psi}_s = S\Omega - b_s \cos\beta_s \sin\psi_s - c \sin(\omega_d t + \psi_N) \qquad (33)$$

where c is derived from relative phase angle terms, we choose $\omega_d \gg \dot{\psi}_{32}$, and ψ_N is a geometry-dependent phase factor [40]. This equation has the same form as (7) which describes dithered operation. Our "dithered" term, $c \sin(\omega_d t + \psi_N)$, however, is not a result of the introduction of some external oscillating component. In this scheme, the strong modes are the gyro modes and the weak modes act as a dither.

To make a numerical estimate of the effective dither amplitude c, we let $\gamma = \gamma_a = \gamma_b = \Delta$. With a gyro operating around

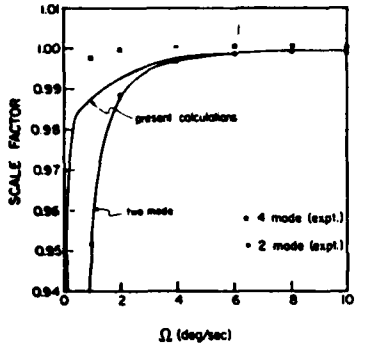

Fig. 22. Normalized scale factor versus input rotation rate for 2+2 configuration. The points are the experimental results, while the curves are obtained by solving (30) and (40) numerically [42].

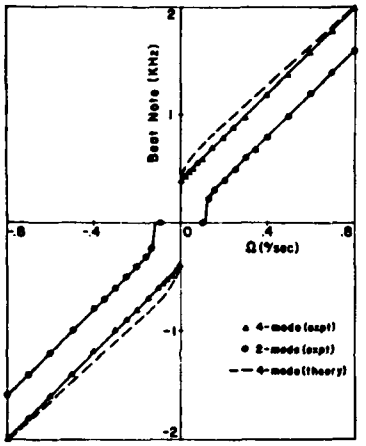

Fig. 23. Beat note versus input rotation rate for a different "2+2" configuration. Here no lock-in region is encountered. The beat note curve for the same gyro operating with two modes is also shown for comparison.

threshold, where the plasma occupies two legs of a triangle and for a cavity bandwidth of about 1 MHz, we find that c is about 0.1-1 kHz when $I_w/I_{sat} \sim 0.01$. Although plausible, this case has not been observed experimentally.

In this dithered scheme the strong modes are well above threshold and the weak modes oscillate weakly with a frequency difference maintained at $\omega_d = \nu_1 - \nu_4$. In other words, we never allow the weak modes to lock. We now remove this restriction. It is seen experimentally [43] that as the two weak off-axial modes are brought above threshold, the lock-in region reduces in width (see Fig. 22). This result is obtained theoretically in [43] by numerically integrating equations of motion for the relative phase angles $\psi\pm = \psi_{32} \pm \psi_{41}$.

More recently, in a similar experiment [44], the lock-in region vanished altogether (see Fig. 23) due to the occurrence of an induced ("2+2") bias much larger than the backscatter contributions. This case is particularly interesting because it consists of a standard two-mode gyro pumped slightly harder than usual, and consequently we discuss it here in somewhat greater detail. The analysis [44] of the vanishing lock-in region and "2+2" bias is very similar to that used by Aronowitz and Lim [46] to explain the positive scale factor correction in two-mode laser gyros. However, the result obtained for the four-mode case is very different.

In our analysis of the amplitude and frequency equations (27) and (28) appropriate for the scalar ring laser, it is convenient to use the following variables:

1) average strong-mode intensity $I_s = (I_3 + I_2)/2$ and weak mode intensity $I_w = (I_4 + I_1)/2$

2) normalized intensity differences $i_s = (I_3 - I_2)/2I_s$ and $i_w = (I_4 - I_1)/2I_w$

3) phases ψ^+ and ψ^-.

Simplifications to the equations may be made by noting that in the experiments the average intensities are constant and the ratios i_s and i_w are small. Furthermore, it was observed that the strong and weak mode beat notes are equal. Using the above information we find the working equations for our problem:

$$\frac{di_s}{dt} = -2\alpha_s i_s + 2b_s \sin \epsilon_s \cos \phi \tag{34}$$

$$\frac{di_w}{dt} = -2'_w i_w - 2\theta_{sw} I_s i_s - 2b_w \sin \epsilon_w \cos \phi \tag{35}$$

$$\frac{d\phi}{dt} = S\Omega + \{b_s i_s \sin \epsilon_s - b_w i_w \sin \epsilon_w\} \sin \phi \tag{36}$$

where $\phi = \psi^+/2$ is the beat note between the strong or the weak counterrotating modes, $\alpha'_w = \alpha_w - \theta_{sw} I_s$, θ_{sw} is the cross-section coefficient between the strong and the weak modes, and all the other variables have been defined earlier. We have allowed for the strong and weak modes to have different backscattering coefficients and phases. In order to have constant total intensity, the backscattering phases ϵ_s and ϵ_w have to be odd multiples of $\pi/2$. Equation (34) may be rewritten in the form

$$i_s = 2b_s \sin \epsilon_s \int dt_1 e^{-2\alpha_s(t-t_1)} \cos \phi(t_1).$$

Since the strong modes are far above threshold, $\alpha_s >> \dot{\phi}$ and the cosine may be taken outside of the integral. One then finds

$$i_s = b_s \frac{\sin \epsilon_s}{\alpha_s} \cos \phi. \tag{37}$$

Equation (4) may also be rewritten in the form

$$i_w = -2Ab_w \sin \epsilon_w \int dt_1 e^{-2\alpha'_w(t-t_1)} \cos \phi(t_1)$$

where

$$A = 1 + \frac{b_s \sin \epsilon_s}{b_w \sin \epsilon_w} \frac{\theta_{sw}}{\beta_s - \theta_s}. \tag{38}$$

In the case of the weak modes it is possible that $\alpha'_w \ll \dot{\phi}$, allowing the exponent to be replaced by unity and

$$i_w = -2A \frac{b_w \sin \epsilon_w}{\dot{\phi}} \sin \phi. \tag{39}$$

By substituting (37) and (39) into (36), we obtain an expression for the "2+2" beat note:

$$\dot{\phi} = S\Omega + Ab_w^2/\dot{\phi} - A\,(b_w^2/\dot{\phi})\cos 2\phi + b_s^2/(2\alpha_s)\sin 2\,\phi. \quad (40)$$

Note that in the absence of the weak modes, (40) reduces to the usual lock-in equation where the lock-in threshold is $|S\Omega| = b_s^2/2\alpha_s$. To determine the effect of the weak modes we solve (40) for $\dot{\phi}$. For the purpose of discussion, we neglect the last term. This is justified because the bias obtained is much greater than $b_s^2/2\alpha_s$. By doing so we have a quadratic equation in $\dot{\phi}$, with a solution

$$\dot{\phi} = S\frac{\Omega}{2} \pm \frac{1}{2}\sqrt{(S\Omega)^2 + 8\,(b_w\sqrt{A})^2\sin^2\phi}. \quad (41)$$

For large positive input rotation rates we expect $\dot{\phi} = S\Omega$. Therefore, only the plus solution is valid for positive rotation. Similarly, only the negative solution is valid for negative rotation. As the rotation rate approaches zero from the positive side, we have

$$\dot{\phi} \simeq b_w\sqrt{2A}\,|\sin\phi|. \quad (42)$$

We see here that the stationary values ($\dot{\phi} = 0$) $\phi = 2n\pi$ are unstable, and therefore no lock-in band is encountered. Phase fluctuations due to, for example, mechanical vibrations kick the system from $\phi = 2n\pi$ points towards $\phi = 2\,(n+1)\,\pi$, but not in the reverse direction. Since (42) shows that the phase can only increase, we obtain a positive bias which may be as big as $b_w\sqrt{2A}$. Similarly, as we approach zero input rotation from the negative side, a negative bias equal in magnitude to the positive bias is encountered.

At this point one may question whether it is really necessary to have four modes. It would seem from our derivation that as long as the excitation is sufficiently low such that $\alpha \ll \dot{\phi}$, an induced bias and a zero lock-in band can be obtained. A closer examination shows that the assumption $\alpha \ll \dot{\phi}$ implies that the two-mode amplitudes differ significantly and in an unstable fashion. In fact, if $\alpha \ll \dot{\phi}$, the two-mode gyro does indeed have

$$i = -2\frac{b_w}{\dot{\phi}}\sin\phi$$

and one gets an equation similar to (39) with $A = 1$. But note that at low input rates (41) gives $\dot{\phi} \simeq b_w$ which leads to $i \simeq 1$. This corresponds to one of the mode intensities being close to zero. In the four-mode case the term $\theta_{sw}I_s$ in (35) causes $i_w \simeq \sqrt{A}$ at zero input rotation. Thus, by making a proper choice of backscattering angles, i.e., $\sin\epsilon_s = -\sin\epsilon_w$, i_w may be made to remain small.

To determine the "2+2" bias, (41) was solved numerically with a computer. The two-mode backscattering contribution was included by replacing $S\Omega$ with $S\Omega + (b_s^2/2\alpha_s)\sin 2\phi$ and a rapidly varying function $F(t)$ was added to ϕ to account for the presence of noise. This function $F(t)$ has a zero time average and a 5 Hz amplitude, which is the uncertainty of the measured beat note. The two-mode lock-in coefficient is measured to be around 250 Hz and this in turn gives $b_w \simeq 10$ kHz. We estimated the intensity variation $i_w \simeq 20$ percent giving $A = 0.04$. Finally, since we have a 40 cm cavity, $S = 2$ kHz/(°/s). The theoretical curve corresponding to these values is shown in Fig. 23 (dashed lines).

In summary, preliminary theoretical investigations lead us to believe that the "2+2" bias may be based on the following features.

1) The nonlinear interaction between the active medium and the four gyro modes gives rise to relative phase angle terms. These terms strongly couple the beat frequencies of the strong and weak modes. As a result the two beat frequencies are locked to each other.

2) Intensities between counterrotating modes vary with the beat note frequency. In the two-mode gyro this variation introduces a bias to the beat note. However, this bias is always less than the lock-in threshold. In the "2+2" gyro there exist experimental configurations where the induced bias is larger than the lock-in threshold.

Further work is required on the "2+2" gyro. Tuning characteristics need to be investigated. Gyro behavior at close to zero input rotation is not clearly understood. Since there is reason to believe that phase fluctuations play a role in creating the bias at very low input rotations, the magnitude and sources of these fluctuations need to be found. Modifications should be made to our theory to account for the fact that at least two of the gyro modes are operating far above threshold. Finally, further investigation into the behavior of the backscattering phases is required.

Appendix I

ZLAG Amplitude- and Frequency-Determining Equations

This appendix expands (25) and (26) to give the eight ZLAG amplitude- and frequency-determining equations, and summarizes the rotation used. Equation (25) expands to

$$\begin{aligned}
\dot{E}_1 &= E_1\,[\alpha_1 - \beta_1 I_1 - \theta_{12}I_2 - \theta_{13}I_3 - \theta_{14}I_4] \\
&\quad - \mathrm{Im}\,[(\vartheta_{1243} + \vartheta_{1342})\,e^{i\psi_{1243}}]\,E_2E_4E_3 \\
&\quad - [Q_{xy}\cos\psi_{12} - \nu_{xy}\sin\psi_{12}]\,E_2 - b_3E_3\cos(\psi_{13} - \epsilon_3) \\
\dot{E}_2 &= E_2\,[\alpha_2 - \beta_2 I_1 - \theta_{21}I_1 - \theta_{23}I_3 - \theta_{24}I_4] \\
&\quad - \mathrm{Im}\,[(\vartheta_{2431} + \vartheta_{2134})\,e^{-i\psi_{1243}}]\,E_4E_3E_1 \\
&\quad - [Q_{xy}\cos\psi_{21} - \nu_{xy}\sin\psi_{21}]\,E_1 - b_4E_4 \\
&\quad \cdot\cos(\psi_{24} - \epsilon_4) \\
\dot{E}_3 &= E_3\,[\alpha_3 - \beta_3 I_3 - \theta_{31}I_1 - \theta_{32}I_2 - \theta_{34}I_4] \\
&\quad - \mathrm{Im}\,[\vartheta_{3124} + \vartheta_{3421})\,e^{-i\psi_{1243}}]\,E_1E_2E_4 \\
&\quad - [Q_{xy}\cos\psi_{34} - \nu_{xy}\sin\psi_{34}]\,E_4 - b_1E_1 \\
&\quad \cdot\cos(\psi_{31} - \epsilon_1) \\
\dot{E}_4 &= E_4\,[\alpha_4 - \beta_4 I_4 - \theta_{41}I_1 - \theta_{42}I_2 - \theta_{43}I_3] \\
&\quad - \mathrm{Im}\,[(\vartheta_{4213} + \vartheta_{4312})\,e^{i\psi_{1243}}]\,E_2E_1E_3 \\
&\quad - [Q_{xy}\cos\psi_{43} - \nu_{xy}\sin\psi_{43}]\,E_3 - b_2E_2 \\
&\quad \cdot\cos(\psi_{42} - \epsilon_2).
\end{aligned}$$

Equation (26) expands to

$$\nu_1 + \dot{\phi}_1 = \Omega_1 + \sigma_1 - \rho_1 I_1 - \tau_{12} I_2 - \tau_{13} I_3 - \tau_{14} I_4 - \mathrm{Re}\,[(\vartheta_{1243} + \vartheta_{1342})\, e^{i\psi_{1243}}]\, E_1^{-1} E_2 E_4 E_3 + \frac{E_2}{E_1}\,[Q_{xy} \sin \psi_{12} + \nu_{xy} \cos \psi_{12}] + b_3 \frac{E_3}{E_1} \sin (\psi_{13} - \epsilon_3)$$

$$\nu_2 + \dot{\phi}_2 = \Omega_2 + \sigma_2 - \rho_2 I_2 - \tau_{21} I_1 - \tau_{23} I_3 - \tau_{24} I_4 - \mathrm{Re}\,[(\vartheta_{2431} + \vartheta_{2134})\, e^{-i\psi_{1243}}]\, E_2^{-1} E_4 E_3 E_1 + \frac{E_1}{E_2}\,[Q_{xy} \sin \psi_{21} + \nu_{xy} \cos \psi_{21}] + b_4 \frac{E_4}{E_2} \sin (\psi_{24} - \epsilon_4)$$

$$\nu_3 + \dot{\phi}_3 = \Omega_3 + \sigma_3 - \rho_3 I_3 - \tau_{31} I_1 - \tau_{32} I_2 - \tau_{34} I_4 - \mathrm{Re}\,[(\vartheta_{3124} + \vartheta_{3421})\, e^{-i\psi_{1243}}]\, E_3^{-1} E_1 E_2 E_3 + \frac{E_4}{E_3}\,[Q_{xy} \sin \psi_{34} + \nu_{xy} \cos \psi_{34}] + b_1 \frac{E_1}{E_3} \sin (\psi_{31} - \epsilon_1)$$

$$\nu_4 + \dot{\phi}_4 = \Omega_4 + \sigma_4 - \rho_4 I_4 - \tau_{41} I_1 - \tau_{42} I_2 - \tau_{43} I_3 - \mathrm{Re}\,[(\vartheta_{4213} + \vartheta_{4312})\, e^{i\psi_{1243}}]\, E_4^{-1} E_2 E_1 E_3 + \frac{E_3}{E_4}\,[Q_{xy} \sin \psi_{43} + \nu_{xy} \cos \psi_{43}] + b_2 \frac{E_2}{E_4} \sin (\psi_{42} - \epsilon_2).$$

We list the notations used below:

E_n = the nth mode electric field amplitude and is slowly varying in time, compared to an optical period

I_n = the dimensionless intensity $(\mathcal{P} E_n/\hbar)^2(\gamma_a^{-1} + \gamma_b^{-1})/2\gamma$

$\dot{E}_n$ = the time derivative of E_n

α_n = the nth mode net linear gain

β_n = the nth mode self-saturation coefficient

θ_{nm} = the nth mode cross saturation coefficient arising from the presence of mode m

ϑ_{nmjk} = a general third-order coefficient

$\nu_n + \dot{\phi}_n$ = the nth mode frequency and $\phi_n(t)$ is a slowly varying phase in the time scale of an optical period

$\psi_{nm} = (\nu_n - \nu_m)\, t + (\phi_n - \phi_m)$

$\psi_{1243} = \psi_{12} + \psi_{43}$

$Q_{xy} = \frac{c}{2L}(l_y - l_x)$ is the x-y Q anisotropy coefficient

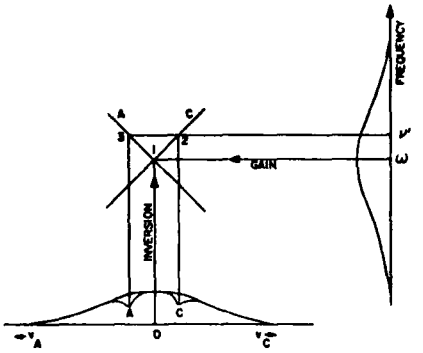

Fig. 24. Yntema diagram for a single isotope. A mode with frequency ν' and anticlockwise direction interacts with the velocity group at A on the abscissa. For clockwise direction, it interacts with the group at C.

$l_x E_X$ and $l_y E_y$ = the losses of the x and y polarized waves per roundtrip

c = the velocity of light

L = the cavity length

$\nu_{xy} = \frac{c}{2L}(\phi_y - \phi_x)$ is the x-y phase anisotropy coefficient

ϕ_x and ϕ_y = the phase shifts added onto the s and p waves per roundtrip

$b_n = \frac{c}{L} r_n$ is the backscattering coefficient

$r_n E_n$ = the increment in the amplitude of the backscattered wave per roundtrip (the nth mode is backscattered)

ϵ_n = the phase shift given to the backscattered part of the wave

Ω_n = the nth mode passive cavity frequency (includes rotation effects)

σ_n = the nth mode frequency pulling term

ρ_n = the nth mode self frequency pushing coefficient

τ_{nm} = the nth mode pushing coefficient arising from the presence of mode m.

Appendix II

Yntema Diagram and Hole Burning

As one can gather by now, due to mode coupling the ZLAG problem has become quite complicated. An analysis of mode competition may be simplified by using the concept of hole-burning. One is then required to translate between mode frequencies and atomic axial velocities. With multimode operation and the presence of several isotopes, this is not straightforward. To facilitate the translation, we use the Yntema diagram.

The Yntema diagram for the case of single isotope and zero detuning is shown in Fig. 24. The abscissa represents the atomic axial velocity with positive values taken anticlockwise. A Gaussian curve of the unsaturated population inversion is

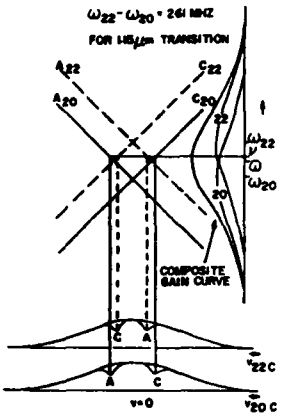

Fig. 25. Yntema diagram for two isotopes. This diagram allows determination of which isotope's velocity group is involved given any mode frequency. Note that there are essentially two Yntema diagrams. Thus, care must be taken to use the population versus velocity curve agreeing with the "reflection" line used.

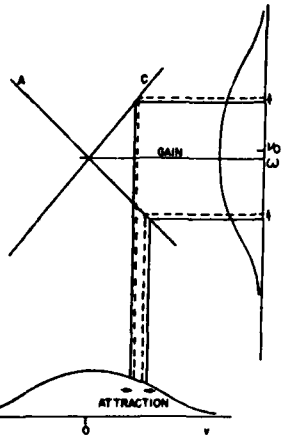

Fig. 26. Illustration of hole attraction. The average frequency $\nu_0 > \omega$ is repelled from ω in frequency space. This translation corresponds to hole attraction in velocity space.

plotted on the abscissa. The ordinate on the right represents optical mode frequencies and has the unsaturated gain plotted on it. With no detuning, a stationary atom ($v = 0$) interacts with the natural atomic frequency ω. Hence, to translate between ω and $v = 0$ we draw a horizontal line from ω that intersects a vertical line drawn from $v = 0$ at point 1. Consider an anticlockwise wave with a frequency $\nu' > \omega$. To interact resonantly with this wave, the atom's motion must downshift ν' to ω in the atomic rest frame. Thus, for this case, the atom must have a velocity in the anticlockwise ($v > 0$) direction. A vertical line is drawn from this velocity so as to intersect a horizontal line drawn from ν' at point 2. A line labeled A is then drawn through points 1 and 2. Now the velocity group that interacts with any anticlockwise wave can be obtained by drawing a vertical line from the point of intersection between line A and the horizontal line from the mode frequency. For a clockwise wave, a similar analysis gives the line labeled C. Line C is used for clockwise waves in the same way that A is used for anticlockwise waves.

The Yntema diagram may be extended to the case of several isotopes. Consider the case of two isotopes such as Ne^{20} and Ne^{22}. Basically, a second diagram is superimposed upon the first (see Fig. 25). The gain curves for each isotope are displaced in frequency space. Thus, each isotope has a separate set of "reflection" lines A and C. Keeping the two population inversions separate allows easy determination of which isotope's holes are involved. Such a multiisotope diagram may be extended to any number of isotopes or Zeeman splitting schemes by the addition of more curves.

Fig. 25 illustrates a couple of important facts about a dual-isotope scalar ring laser tuned midway between isotropic line centers [$\nu = (\omega_{22} + \omega_{20})/2$]. First, note that because ν is very detuned from either line center, the counterrunning waves interact with essentially different velocity groups, and hence are weakly coupled. Second, the dispersion contributions for the two isotopes have opposite signs and nearly cancel each other.

At this point it is possible to obtain a counter example to the well known statement that "two holes always to tend to repel each other." This case is important in the interpretation of the gyro beat frequency equations. Consider a scalar-field two-mode ring laser with a medium described by the Doppler limit. The corresponding frequency-determining equation is

$$\nu_A + \dot{\phi}_A \simeq \Omega_A' + \sigma_A - \rho_A E_A^2 - \tau_{AC} E_C^2$$

where the cross-pushing coefficient is given by [18]

$$\tau_{AC} = \beta_A [(\omega - \nu)/\gamma] L (\omega - \nu). \tag{10}$$

β_A is the self-saturation coefficient for the anticlockwise wave and $\nu = (\nu_A + \nu_C)/2$. Notice that it is the mean frequency ν that is pushed away from line center. For modes on opposite sides of the line center, the mode on the ν side is pushed and the other mode is pulled. The net effect is a linear translation of the two modes. Fig. 26 shows that this linear translation of ν gives hole repulsion or attraction in velocity space depending on the sign of $(\omega - \nu)$.

We conclude this section by making a few observations about hole burning. First, a wave draws power from the atoms with which it is resonant and tends to saturate the population difference. Since the atoms have a finite homogeneous linewidth, the wave burns a hole into the population difference. To a good approximation this is described by a Bennett hole, which is Lorentzian in shape. This approximation neglects the fact that two or more waves generate population pulsations that modify the inversion described by the Bennett hole.

The second point is that it is important to realize that the atomic gain is not directly proportional to the population difference (the number of inverted atoms per unit volume, per unit velocity). This is because the atoms have a finite lifetime so that a wave actually samples atoms from several velocity groups. Thus, the gain is given by the convolution of the homogeneous lineshape with the population difference [37], [49], [48]. For the unsaturated case and a Gaussian in-

homogeneous distribution, this convolution is the plasma dispersion function $Z(\nu)$. Its imaginary part determines the gain and resembles a Gaussian with Lorentzian wings. In the limit that the linewidth of the atoms goes to a delta function, this function returns to a Gaussian. The saturated population difference, in turn, gives a gain that is equal to the convolution of the homogeneous lineshape with the saturated population difference. As such, it is important to remember that a hole in the population versus velocity curve does not transform to an equivalent hole in the gain curve merely by reflection from the A and C lines in the Yntema diagram. In particular, the gain for a single saturating wave has no holes versus frequency. The gain for a nonsaturating wave that probes the medium in the vicinity of a saturating wave has a Lorentzian hole, but with width $2(\gamma + \gamma')$, where 2γ is the natural linewidth and $2\gamma'$ is the power-broadened value [48]. This is because the convolution of two Lorentzians is a Lorentzian with the sum of the widths.

References

[1] C. V. Heer, "Interference of electromagnetic and matter waves in a nonpermanent gravitational field," *Bull. Amer. Phys. Soc.*, vol. 6, p. 58, 1961.

[2] A. Rosenthal, "Regenerative circulatory multiple beam interferometry for the study of light propagation effects," *J. Opt. Soc. Amer.*, vol. 52, pp. 1143-1148, 1962.

[3] —, U.S. Patent 3 332 314, 1967.

[4] W. M. Macek and D. T. M. Davis, Jr., "Rotation rate sensing with traveling-wave ring lasers," *Appl. Phys. Lett.*, vol. 2, pp. 67-68, 1963.

[5] F. Aronowitz, "The laser gyro tutorial review," *Proc. SPIE*, vol. 157, pp. 2-6, 1978.

[6] K. Thomson, "Integrated 3-axis laser gyro," *Proc. SPIE*, vol. 157, pp. 13-20, 1978.

[7] G. Sagnac, *C. R. Acad. Sci.*, vol. 157, p. 708, 1913.

[8] E. J. Post, "Sagnac effect," *Rev. Mod. Phys.*, vol. 39, pp. 475-493, 1967.

[9] J. Killpatrick, "The laser gyro," *IEEE Spectrum*, vol. 4, pp. 44-55, 1967.

[10] T. J. Hutchings and D. C. Stjern, "Scale factor nonlinearity of a body dither laser gyro," in *Proc. IEEE 1978 Nat. Aerospace and Electron. Conf.*, pp. 549-543.

[11] F. Aronowitz, "The laser gyro," in *Laser Applications*, M. Ross, Ed. New York: Academic, 1971, pp. 113-200.

[12] F. Aronowitz and R. J. Collins, "Lock-in and intensity-phase interaction in the ring laser," *J. Appl. Phys.*, vol. 44, pp. 130-141, 1970; —, "Mode coupling due to backscattering in a He-Ne traveling wave ring laser," *Appl. Phys. Lett.*, vol. 9, pp. 55-58, July 1966.

[13] F. Aronowitz, "Loss lock-in in the ring laser," *J. Appl. Phys.*, vol. 41, pp. 2453-2456, 1970.

[14] G. Yntema, D. Grant, Jr., and R. Warner, U.S. Patent 3 862 803, 1975.

[15] K. Andringa, U.S. Patent 3 930 731, 1976.

[16] D. R. Hanson and M. Sargent III, "Theory of a Zeeman ring laser: General formalism," *Phys. Rev.*, vol. A9, pp. 466-480, 1974.

[17] D. Grant, J. B. Hambenne, T. J. Hutchings, V. Sanders, and M. O. Scully, "A multioscillator (four mode) ring laser gyro report," *NAECON 1977 Record*, pp. 1028-1032.

[18] W. W. Chow, J. B. Hambenne, D. R. Hanson, M. Sargent III, and M. O. Scully, "Theory of a Zeeman ring laser. Part II—Special cases," *IEEE J. Quantum Electron.*, vol. QE-15, pp. 1301-1309, Nov. 1979.

[19] M. Sargent III, W. E. Lamb, Jr., and R. L. Fork, "Theory of a Zeeman Laser. I," *Phys. Rev.*, vol. 164, pp. 436-449, 1967; —, "Theory of a Zeeman Laser. II," *Phys. Rev.*, vol. 164, pp. 450-465, 1967.

[20] W. J. Tomlinson and R. L. Fork, "Properties of gaseous optical masers in weak axial magnetic fields," *Phys. Rev.*, vol. 164, pp. 466-483, 1967.

[21] T. J. Hutchings, J. Winocur, R. H. Durrett, E. D. Jacobs, and W. L. Zingery, "Amplitude and frequency characteristics of a ring laser," *Phys. Rev.*, vol. 152, pp. 467-473, 1966.

[22] F. Aronowitz, "Theory of a traveling wave optical maser," *Phys. Rev.*, vol. 139, pp. A635-A646, 1965.

[23] A. L. Schawlow and C. H. Townes, "Infrared and optical masers," *Phys. Rev.*, vol. 112, pp. 1940-1949, 1958.

[24] M. O. Scully and W. E. Lamb, Jr., "Quantum theory of an optical maser," *Phys. Rev. Lett.*, vol. 16, pp. 853-855, 1966.

[25] A. Javan, E. A. Ballik, and W. L. Bond, "Frequency characteristics of a continuous wave He-Ne optical maser," *J. Opt. Soc. Amer.*, vol. 52, pp. 96-98, 1968.

[26] F. Aronowitz, "Single-isotope laser gyro," *Appl. Opt.*, vol. 11, pp. 405-412, 1972; —, Effects of radiation trapping on mode competition and dispersion in the ring laser," pp. 2146-2152, 1972.

[27] J. A. White, "Stability of traveling waves in lasers," *Phys. Rev.*, vol. 137, pp. A1651-A1654, Mar. 1965.

[28] J. B. Hambenne and M. Sargent, III, "Physical interpretation of bistable unidirectional ring-laser operation," *IEEE J. Quantum Electron.*, vol. QE-11, pp. 90-92, Feb. 1975.

[29] W. M. Macek and E. J. McCartney, *Sperry Rand Eng. Rev.*, vol. 1, p. 8, 1966.

[30] P. H. Lee and J. G. Atwood, "Measurement of saturation induced optical nonreciprocity in a ring laser plasma," *IEEE J. Quantum Electron.*, vol. QE-2, pp. 235-243, May 1966.

[31] W. Stowell, "A precision measurement of Fresnel drag in a ring laser," Ph.D. dissertation, Oklahoma State Univ., July 1974.

[32] R. E. McLure and E. Vaher, "An improved ring laser bias element," in *Proc. IEEE 1978 Nat. Aerospace and Electron. Conf.*, pp. 544-548.

[33] H. Boot, P. King, and R. Shersby-Harole, "Ring laser bias using reciprocal optical components," *Electron. Lett.*, vol. 5, pp. 347-348, July 1969.

[34] J. D. Coccoli and J. R. Lawson, U.S. Patent 3 533 014, Oct. 1970.

[35] H. deLang, "Polarization properties of optical resonators passive and active," Ph.D. dissertation, Univ. Utrecht, 1966.

[36] W. E. Lamb, Jr., "Theory of an optical maser," *Phys. Rev.*, vol. 134, pp. A1429-A1450, 1964.

[37] M. Sargent, III, M. O. Scully, and W. E. Lamb, Jr., *Laser Physics*. Reading, MA: Addison-Wesley, 1974.

[38] T. A. Dorschner and I. W. Smith, "Clear path four frequency resonators for ring laser gyros," *J. Opt. Soc. Amer.*, vol. 68, p. 1381, 1978.

[39] I. W. Smith and T. A. Dorschner, "Electromagnetic wave ring resonator," U.S. Patent 4 110 045, Aug. 1978.

[40] G. S. Kruglik and A. A. Kutsak, "Effect of multiple modes on the beats in a ring laser," *Zhurnal Prikladnoi Spektroskoppi*, vol. 14, pp. 59-64, 1971.

[41] M. O. Scully, V. Sanders, and M. Sargent III, "Novel multioscillator approach to the problem of locking in the two-mode ring-laser gyro," *Opt. Lett.*, vol. 3, pp. 43-45, 1978.

[42] V. Sanders, D. Anderson, and M. O. Scully, "A four mode solution to the locking problem in two-mode ring laser gyro," presented at the 22nd Int. Symp. Laser Inertial Rotation Syst., 1978.

[43] D. Anderson, W. W. Chow, V. Sanders, and M. O. Scully, "Novel multioscillator approach to the problem of locking in 2 mode ring laser gyros: II," *Appl. Opt.*, vol. 18, pp. 941-942, 1979.

[44] D. Anderson, W. W. Chow, M. O. Scully, and V. Sanders, "A reciprocally biased four-mode ring laser gyro," to be published.

[45] C. L. O'Bryan, III and M. Sargent III, "Theory of multimode laser operation," *Phys. Rev.*, vol. A8, pp. 3071-3092, 1973.

[46] F. Aronowitz and W. L. Lim, "Positive scale factor correction in the laser gyro," *IEEE J. Quantum Electron.*, vol. QE-13, pp. 388-343, Apr. 1977.

[47] W. R. Bennett, Jr., "Some aspects of the physics of gas lasers," in *Brandeis University Summer Institute in Theoretical Physics, 1969*, M. Chretien and S. Lipworth, Eds. New York: Gordon and Breach, 1971, pp. 5-201.

[48] See, for example, M. Sargent III, "Spectroscopic techniques based on Lamb's laser theory," *Phys. Rep.*, vol. 43, pp. 223-265, 1978.

APPENDIX D

A PROPOSED OPTICAL TEST OF PREFERRED FRAME COSMOLOGIES *

Mark P. HAUGAN [1], Marlan O. SCULLY and Kurt JUST
Theoretical Physics Division and Optical Sciences Center, University of Arizona, Tucson, AZ 85721, USA
and Projektgruppe für Laserforschung der Max-Planck-Gesellschaft, D-8046 Garching bei München, West Germany

Received 12 March 1980

We propose a new experiment employing an earthbound ring laser interferometer to search for evidence of a preferred frame in the Universe. It would yield a measurement of or a tight new constraint on the value of the PPN parameter α_1.

An important class of experiments testing the foundations of gravitation theory search for evidence of a preferred reference frame in the Universe [1,2]. In this letter we propose a new optical test [3] of metric gravitation theories that would be sensitive to the presence of a preferred frame. The experiment would employ a ring laser interferometer in an earthbound laboratory. We show that in the context of the PPN formalism, [1;4, ch. 39] which was developed to provide a means for studying general metric theories of gravity in the weak-field, slow-motion setting of the solar system, a ring laser device is sensitive to the value of the preferred-frame parameter α_1, the weakest point in the present empirical knowledge of post-newtonian gravitation. We know only that $|\alpha_1| \leqslant 0.02$, while general relativity predicts $\alpha_1 = 0$. Experimental considerations suggest that a ring interferometer experiment to measure or to place tight new limits on the value of α_1 is practicable. Here, we will discuss the detectability of the possible preferred-frame signal only briefly. The reader is referred to a longer paper, in preparation, for a deeper analysis [5].

In the next few paragraphs we analyze and discuss the generalized Sagnac effect in a form appropriate to the present problem. It shows that the beat note between the counter-running wave [6] in a ring laser [7] is affected not only by the rotation of the earth and by nonreciprocal elements, but also by off-diagonal gravitational contributions to the line element in the interferometer's frame. To this end we summarize the calculations of the optical beat note that would be observed in a ring laser situated in the earth's gravitational field.

The covariant form of Maxwell's equations for the vector potential $A_\sigma(x^\mu)$ is

$$\partial_\nu[\sqrt{-g}\,g^{\mu\rho}g^{\nu\sigma}(\partial_\sigma A_\rho - \partial_\rho A_\sigma)] = 0\,, \quad g = \det g_{\mu\nu}\,. \tag{1}$$

To determine the frequency difference between the two counter-propagating laser beams we write the metric as $g_{\mu\nu} = \eta_{\mu\nu} + h_{\mu\nu}$, where $\eta_{\mu\nu}$ is that of flat spacetime and $h_{\mu\nu}$ a small correction due to the earth's gravitational field and the rotation of the ring. We can always construct coordinates with respect to which $h_{\mu\nu} = 0$ at the center of the ring laser. In these coordinates, $h_{\mu\nu}$ will be small throughout the region containing the interferometer. The smallness of the laser wavelength relative to the scale on which the gravitational field varies, the size of the ring, and the laser beam width implies that the high frequency limit [8] of the Maxwell equations suffices to determine A_μ [‡1].

* This work is supported in part by the Air Force Office of Scientific Research (AFSC), United States Air Force, the Army Research Office, United States Army and the National Science Foundation under grant PHY78-05368.

[1] Permanent address: Department of Physics, University of Utah, Salt Lake City, UT 84112, USA.

[‡1] We have obtained corrections to our high-frequency analysis that arise due to finiteness of the smallest instrumental scale, that of the laser beam width [9].

Thus we write $A_\mu = \mathscr{A}_\mu \exp[i(S^{(0)} + \Delta S)]$, where $\mathscr{A}_\mu$ is a slowly varying amplitude function and $S^{(0)} + \Delta S$ a rapidly varying phase. The function $S^{(0)}$ is the phase for the case $h_{\mu\nu} \equiv 0$. Solving for ΔS to first order in $h_{\mu\nu}$, we obtain for the frequency difference between the counter-running waves:

$$\Delta\omega = \frac{2}{\lambda\!\!\!^{-}P} \iint_{\Sigma} (\nabla \times \boldsymbol{h}) \cdot \mathrm{d}\boldsymbol{a} \approx \frac{2A}{\lambda\!\!\!^{-}P} (\nabla \times \boldsymbol{h}) \cdot \hat{\boldsymbol{z}} , \qquad (2)$$

where $(\boldsymbol{h})_i \equiv h_{0i}$. While $\lambda\!\!\!^{-}$ is the reduced wavelength, A and P are the area and perimeter of the planar surface bounded by the ray path of the interferometer; $\hat{\boldsymbol{z}}$ is a unit vector normal to the plane of the device, i.e., that points in the direction of its axis. The surface Σ is one bounded by the ray path and the curl is evaluated at the center of the interferometer. When the ring spins on its axis with angular rate Ω in the absence of gravity, the result (2) becomes $\Delta\omega = 4A\Omega/\lambda\!\!\!^{-}P$, which gives the usual Sagnac effect.

We now turn to the PPN formalism to determine the value of (2) in the presence of gravity. We construct an explicit transformation from the PPN coordinate system centered on the earth (and rotationally tied to the fixed stars) to a system in which the interferometer is at rest and in which the metric has $h_{\mu\nu} = g_{\mu\nu} - \eta_{\mu\nu} = 0$ at the center of the ring. The expression for $h_{\mu\nu}$ in these coordinates is then used to evaluate (2). We obtain

$$\nabla \times \boldsymbol{h} = 2[\boldsymbol{\Omega}_\oplus + \tfrac{1}{4}\alpha_1 \boldsymbol{w} \times \nabla U - (\gamma + 1)\boldsymbol{v} \times \nabla U - \tfrac{1}{4}(7\Delta_1 + \Delta_2)\boldsymbol{\Delta} \times \boldsymbol{V}] , \qquad (3)$$

where the derivatives of U and $\boldsymbol{V}$, potentials in the PPN coordinates [‡2] determined by the density and velocity distribution of matter in the earth, are to be evaluated at the interferometer's center; $\boldsymbol{v}$ is the laboratory velocity through the PPN coordinates due to the earth rotation $\boldsymbol{\Omega}_\oplus$; and $\boldsymbol{w}$ is the velocity of the earth relative to fixed stars, i.e., relative to the frame in which the cosmic microwave background appears isotropic. For the present discussion, it is sufficient to treat the earth as a uniform, rigidly rotating sphere. Eqs. (2) and (3) imply that an interferometer at latitude l spinning about its axis in the lab, $\hat{\boldsymbol{z}} = (\cos\theta_\xi, \cos\theta_\eta, \cos\theta_\zeta)$, at rate Ω_0 will exhibit a frequency difference

$$\Delta\omega = (4A/\lambda\!\!\!^{-}P)\{\Omega_0 + \Omega_\oplus \cos\theta_\zeta + \tfrac{1}{8}\alpha_1(r_s/r_\oplus^2)|w|[(A(t_s)\sin l - C\cos l)\cos\theta_\xi - B(t_s)(\sin l\cos\theta_\eta + \cos l\cos\theta_\zeta)] + \epsilon\} , \qquad (4)$$

where r_s and $r_\oplus$ are the earth's Schwarzschild and actual radii; Ω_0 and $\Omega_\oplus$ are rates of rotation measured by clocks in the laser laboratory, and ϵ stands for a remainder of smaller terms due to such effects as the geodetic and Lense–Thirring rotations [4, §40.7]. The direction $\hat{\boldsymbol{\zeta}}$ coincides with the earth's axis, $\hat{\boldsymbol{\xi}}$ is directed along the velocity associated with the earth's rotation, i.e., "east", and $\hat{\boldsymbol{\eta}} = \hat{\boldsymbol{\zeta}} \times \hat{\boldsymbol{\xi}}$. According to measurements of the dipolar anisotropy of the cosmic microwave background by Smoot et al. [10,11],

$$|w| = (390 \mp 60)\ \mathrm{km/s} ,$$

$$A(t_s) = \cos\delta\cos\alpha , \quad B(t_s) = \cos\delta\sin\alpha ,$$

$$C = \sin\delta , \quad \delta = 6^\circ \pm 10^\circ ,$$

$$\alpha = \Omega_\oplus[t_s - (11 \pm 0.6)\ \mathrm{h}] ,$$

where t_s is the sidereal time.

Let us now turn to a brief discussion of the detectability of the α_1-dependent preferred-frame signal described by eq. (4). For optimized latitude and orientation of the interferometer ring, the amplitude of this periodic rotation rate signal is $1.2 \times 10^{-7}\ \alpha_1 \Omega_\oplus$. The most promising experimental approach to its detection employs a passive device with a laser located outside a ring interferometer. This method avoids the "locking" problem associated with active systems in which the lasing medium is situated inside the ring resonator. It also allows larger rings in practice because complicated multi-mode laser oscillation is no longer a problem. Very encouraging estimates of the sensitivity of these passive devices have been offered. For example, the following quote from the recent paper of Ezekiel et al. [12]: "With a $10 \times 10\ \mathrm{m}^2$ cavity and a 4 W stabilized argon laser it should be possible to reach a sensitivity of 10^{-10} of earth rate in an integration time of 1000 s". This sensitivity is estimated by invoking the photon shot noise limit of heterodyne detection. Special notice should be taken of the time required to make a measurement. It is so short that full advantage can be taken of the preferred-frame signal's sidereal periodicity. Phase-sensitive analysis of the interferometer out-

[‡2] These potentials are defined in, for example, refs. [1] and [4, ch. 39].

put will facilitate the separation of this signal from other effects contributing to $\Delta\omega$. A detailed analysis of instrumental, seismic, and other potential noise contributions will be presented in a later paper [5].

It should be remarked that motivation to undertake the development of a ring interferometer system of the type described above does not come only from gravitation physics. Indeed, the consideration of such systems has previously been motivated by potential geophysical applications (e.g., measurements of earth wobble, of rotational seismic motions, etc.) and by the need for high precision test equipment for turntables and gyroscopes. The opportunity to perform a significant gravitational experiment does, however, make an interesting and important addition to such applications.

In summary, the experiment we describe would employ a high precision ring laser interferometer ($10^{-10}\,\Omega_\oplus$ sensitivity) with good time resolution (10^3 s to make a measurement) to search for a sidereal periodic effect due to a possible preferred frame in the Universe. A device with the above characteristics would be able to set a limit $|\alpha_1| \lesssim 10^{-3}$, more than an order of magnitude improvement on the present limit.

References

[1] C.M. Will and K. Nordtvedt Jr., Astrophys. J. 177 (1972) 757, 775.
[2] M.P. Haugan, Ann. Phys. (NY) 118 (1979) 156.
[3] Aspects of this work are discussed in: M. Scully, Suggestion and analysis for a new optical test of general relativity, in: Proc. 5th Intern. Conf. on Laser spectroscopy, eds. H. Walther and K. Rothe (Springer, 1979).
[4] See for example, C.W. Misner, K.S. Thorne and J.A. Wheeler, Gravitation (Freeman, San Francisco, 1973); or C.M. Will, in: Einstein centenary volume (Cambridge U.P., Cambridge, 1979).
[5] M. Scully, M.S. Zubairy and M.P. Haugan, in preparation.
[6] See for example, E.J. Post, Rev. Mod. Phys. 39 (1967) 475.
[7] See for example, M. Sargent, M. Scully and W. Lamb, Laser physics (Addison-Wesley, 1974) Ch. 12.
[8] J. Plebanski, Phys. Rev. 118 (1960) 1369.
[9] M.S. Zubairy, M. Scully and K. Just, to be published.
[10] G.F. Smoot, M.V. Gorenstein and R.A. Muller, Phys. Rev. Lett. 39 (1977) 898.
[11] G.F. Smoot and P.M. Lubin, Astrophys. J. 234 (1979) L83.
[12] S. Ezekiel, J.A. Cole, J. Harrison and G. Sanders, SPIE 157 (1978) 68.

☆U.S.Government Printing Office: 1981 — 757-002/395


LME